UPPSALA
UNIVERSITET

UPTEC W 19 040
Examensarbete 30 hp
Juni 2019

The influence of storm movement and temporal variability of rainfall on urban pluvial flooding

1D-2D modelling with empirical hyetographs and CDS-rain

Jimmy Olsson

ABSTRACT

The influence of storm movement and temporal variability of rainfall on urban pluvial flooding – 1D-2D modelling with empirical hyetographs and CDS-rain

Jimmy Olsson

Pluvial floods are formed directly from surface runoff after extreme rain events. Urban areas are prone to suffer from these floods due to large portions of hardened surfaces and limited capacity in the stormwater infrastructure. Previous research has shown that catchment response is influenced by the spatio-temporal behaviour of the rainstorm. A rainstorm moving in the same direction as the surface flow can amplify the runoff peak and temporal variability of rainfall intensity generally results in greater peak discharge compared to constant rainfall. This research attempted to relate the effect of storm movement on flood propagation in urban pluvial flooding to the effect from different distributions of rainfall intensity. An additional objective was to investigate the flood response from recent findings on the temporal variability in Swedish rain events and compare it to the flood depths produced by a CDS-rain (Chicago Design Storm), where the latter is the design practice in flood modelling today.

A 2D surface model of an urban catchment was coupled with a 1D model of the drainage network and forced by six different hyetographs. Among them were five empirical hyetographs developed by Olsson et al. (2017) and one a CDS-rain. The rainstorms were simulated to move in different directions: along and against the surface flow direction, perpendicular to it and with no movement. Maximum flood depth was evaluated at ten locations and the model results show that storm movement had negligible effect on the flood depths. The impact from the movement was likely limited by the big difference in speed between the rainstorm and the surface flow.

All evaluated locations showed a considerable sensitivity to changes in the hyetograph. The maximum flood depth increased at most with a factor of 1.9 depending on the hyetograph that was used as model input. The CDS-rain produced higher flood depths compared to the empirical hyetographs, although one of the empirical hyetographs produced a similar result. Based on the results from this case study, it was concluded that storm movement was not as critical as the temporal variability of rainfall when evaluating maximum flood depth.

Key words: Pluvial flooding, flood modelling, 1D-2D modelling, MIKE FLOOD, MIKE 21, MIKE URBAN, storm movement, temporal variability, hyetograph, design storm, Chicago Design Storm, CDS-rain.

Department of Earth Sciences, Program for Air, Water and Landscape Science, Uppsala University, Villavägen 16, SE-75236 Uppsala, Sweden.

REFERAT
Påverkan från regnmolns rörelse och regnintensitetens variation på urbana pluviala översvämningar – Hydraulisk modellering med empiriska regntyper och CDS-regn
Jimmy Olsson

Pluviala översvämningar skapas från ytavrinning vid intensiva nederbördstillfällen. De uppstår ofta i urbana miljöer till följd av den höga andelen hårdgjorda ytor och ledningsnätets begränsade kapacitet. Forskning har visat att ett regnmolns rörelseriktning och hastighet påverkar avrinningsförloppet. Om molnet rör sig längs med flödesriktningen i terrängen kan en ökning i vattenlödet nedströms ett avrinningsområde uppstå. Denna effekt har visat sig vara störst om hastigheten hos regnmolnet och vattenflödet är likvärdiga. Ytterliggare en faktor som påverkar avrinningsförloppet är hur regnintensiteten är fördelad över tid. Olsson et al. (2017) har tagit fram fem empiriska regntyper som speglar tidsfördelning inom ett Svenskt regntillfälle. Inom översvämningsmodellering är det vanligt att använda ett så kallat CDS-regn (Chicago Design Storm), vilken har en given tidsfördelning. Med anledning av detta är det intressant att jämföra översvämningar genererade av ett CDS-regn och av de empiriska regntyperna.

Syftet med denna studie var att utreda hur regnmolns rörelse påverkar urbana pluviala översvämningar med avseende på vattendjup, samt att jämföra denna påverkan med effekten från olika tidsfördelningar av regnintensiteter. En kombinerad dagvattenmodell (1D) och markavrinningsmodell (2D) av en mindre svensk tätort användes för att simulera olika regnscenarier. De fem empiriska regntyperna och ett CDS-regn simulerades med en rörelseriktning längs med, emot och vinkelrätt i förhållande till flödesriktningen. Även scenarier med stationära regnmoln simulerades. Maximala översvämningsdjup utvärderades i tio punkter spridda över hela modellområdet.

Resultatet från simuleringarna visade att regnmolnets rörelse hade försumbar påverkan på översvämningsdjupen. De olika tidsfördelningarna av regnintensitet hade däremot betydande påverkan på de maximala översvämningssdjupen. Som mest var det det maximala översvämningsdjupet 1.9 gånger större beroende vilken regntyp som användes som indata. CDS-regnet genererade i regel de största översvämningsdjupen, även om utfallet från en av de fem empiriska regntyperna var förhållandevis likvärdigt. Regnintensitetens tidsfördelning var därmed en kritisk parameter vid den hydrauliska modelleringen av urbana pluviala översävmningar, till skillnad från molnrörelse som hade försumbar påverkan.

Nyckelord: Pluviala översvämningar, översvämningsmodellering, 1D-2D modellering, MIKE FLOOD, MIKE 21, MIKE URBAN, molnrörelse, hyetograf, typregn, Chicago Design Storm, CDS-regn.

Institutionen för geovetenskaper, Luft- vatten- och landskapslära, Uppsala universitet, Villavägen 16, 75236 Uppsala, Sverige.

PREFACE

This master thesis is finalizing the Master Programme in Environmental and Water Engineering at Uppsala University and the Swedish University of Agricultural Science. The thesis project corresponds to 30 credits and has been conducted in collaboration with Tyréns, where Johan Kjellin has been supervising. Maurizio Mazzoleni has been subject reader and Björn Claremar examinor, both at the Department of Earth Sciences, Program for Air, Water and Landscape Sciences, Uppsala University.

I would like to direct a special thank you to Johan Kjellin - your inspiring commitment and many inputs have been very helpful for the thesis. Thanks to Gunnar Svensson (Tyréns) and Kalmar Municipality for providing the model and to Sten Blomgren at DHI for the software license. Also, thanks to Jonas Olsson and Johan Södling at SMHI for showing interest in the work and providing data on the empirical hyetographs. Lastly, a huge thanks to Åsa Söderqvist, friends and family for the great support during the work.

Uppsala, June 2019

Jimmy Olsson

UPTEC W 19 040, ISSN 1401-5765.
Published digitally by the Department of Earth Sciences, Uppsala University,
Uppsala, 2019.

POPULÄRVETENSKAPLIG SAMMANFATTNING

Översvämningar kan uppstå när vattennivån i en flod stiger så högt att vattnet flödar ut över omkringliggande mark. De kan också skapas till följd av ett kraftigt skyfall över ett urbant område när regnvolymen är så stor och regnet faller så snabbt att ledningssystemet inte klarar av att avleda det. Vattnet som samlas i olika delar av området härstammar då inte från ett vattendrag utan kommer direkt ifrån regnet. Denna typ av översvämning kallas *pluvial* och är särskilt kritisk då den kan inträffa mycket plötsligt och i områden som normalt inte förknippas med översvämningar.

Det har sedan länge forskats på hur regnmolns rörelse påverkar flöden i vattendrag. Forskare har visat att om molnet rör sig längs med flödesriktningen kan en ökning av flödet ske nedströms. Samma fenomen har påvisats för flöden i dagvattensystem, vilket är ledningar avsedda att avleda regn- och smältvatten. Effekten har visat sig vara som störst då hastigheten hos regnmolnet och vattenflödet är ungefär lika stora. Vidare har man funnit att ett regnförlopp som varierar i intensitet, exempelvis att en kort intensiv period av regn följs av lättare regn, generellt leder till större flöden än om regnet har konstant intensitet. Effekter från olika regnmönster har uppenbarligen studerats tidigare, men hur stora de olika effekterna är på pluviala översvämningar är mindre känt, vilket denna studie syftade till att undersöka.

Forskare vid SMHI har nyligen studerat ett stort antal svenska regn. De tog fram fem empiriska regntyper som speglar hur regnet typiskt är fördelat över tid. Vid modellering av översvämningar är det vanligt att simulera ett så kallat CDS-regn (Chicago Design Storm). Fördelningen av regnet över tid i ett CDS-regn speglar inte ett verkligt regntillfälle, men det har en karakteristisk form. Därför är det intressant att studera skillnaderna mellan översvämningar genererade av de empiriska regntyperna och av CDS-regnet.

För att studera pluviala översvämningar skapade av de olika regnmönsterna användes en modell som beskriver dagvattensystemet och terrängen i den svenska tätorten Smedby, som ligger strax väster om Kalmar. I modellen med dagvattensystemet fanns ledningar och brunnar, medan terrängmodellen representerade bland annat byggnader, vägar och de olika jordtyperna i området. De fem empiriska regntyperna och ett CDS-regn modellerades som kraftiga skyfall, dels utan rörelse och dels med rörelseriktning längs med, emot respektive vinkelrätt mot flödesriktningen i området. Sedan utvärderades maximala översvämningsdjup i tio olika punkter som analyserades med avseende på regntyp och de olika rörelseriktningarna.

Resultatet visade att översvämningsdjupen påverkades mycket lite av regnmolnets rörelse. Den relativa skillnaden i översvämningsdjup då ett regnmoln stod stilla jämfört med när det rörde sig nedströms var i de flesta fall mindre än 0.5%. Detta motsvarar en skillnad på ett par millimeter om översvämningsdjupet är en halvmeter. I de allra flesta fall genererade ett stationärt regnmoln något högre översvämningsdjup, men skillnaden var oftast mindre än 1 millimeter. Det fanns indikationer på att en rörelseriktning nedströms genererade högre översvämningsdjup jämfört med när molnet rörde sig uppströms, men skillnaderna var som sagt mycket små.

Till skillnad från molnets olika rörelseriktningar hade regnets tidsfördelning en betydande inverkan på översvämningsdjupen. I en utvärderingspunkt var vattendjupet från ett typregn nästan dubbelt så stort jämfört med ett annat. De största djupen genererades av CDS-regnet. En av de empiriska regntyperna som SMHI tagit fram genererade liknande djup som CDS-regnet, men vattendjupen från de resterande fyra regntyperna var betydligt lägre. Det finns därför en risk att översvämningsdjupen överskattas om ett CDS-regn används vid modellering av urbana översvämningar.

Resultatet från simuleringarna visade att regnintensitetens fördelning över tid är en viktig parameter när urbana pluviala översvämningar studeras. Däremot finns det inget i denna studie som indikerar att regnmolnens rörelse bör modelleras eftersom denna inverkan var försumbar.

CONTENTS

1 INTRODUCTION

The future poses many challenges in terms of increasing flood risks. Extreme rainfalls are projected to be intensified due to climate change, increasing the probability for floods (Bai et al., 2019). Climate models indicate a future increase of the extreme rainfall depths in Sweden between 10% and 40% (Olsson et al., 2017). Urbanization is another related phenomenon which affect flood risk. The greater part of urban areas consists of impervious surfaces which prevent the water from infiltrate and instead diverts it into the stormwater drainage system (Hernebring & Mårtensson, 2013). This leads to higher runoff rates compared to undeveloped areas and sets high demands on infrastructure planning and design. However, the drainage capacity is limited and the collection system will be surcharged in case of too extreme flows. Drainage networks are not designed to cope with extreme flows, making the mapping of potential hazard areas important. Urban areas are also more prone to suffer from economic cost compared to rural areas, which has become a rising concern globally (Jha et al., 2012). This issue is especially relevant in Sweden, where 87% of the inhabitants lived in urban areas by the end of 2017 (SCB, 2018a). And indeed, Swedish cities have suffered from severe floods in recent years. In 2014 for example, a series of cloudbursts caused floods in many regions and Malmö, Sweden's second largest city, was hit the worst (Hernebring et al., 2015). The resulting insurance claims following the Malmö event amounted to more than SEK 300 million (Hernebring et al., 2015). A detailed knowledge of the processes behind urban pluvial flooding is therefore of great importance, which is something this study will take an approach on.

Hydraulic modelling is a common approach to study different urban flooding phenomena (Hernebring & Mårtensson, 2013). A so-called design storm is oftentimes used as model input and the Chicago Design Storm (CDS-rain) is common in Swedish flood simulations (Svenskt Vatten, 2011). Olsson et al. (2017) recently developed empirical hyetographs (rainfall intensity vs. time) based on historical rain data from gauges in Sweden. It would therefore be of interest to study how the flooding consequences differs between an established design practice and the findings by Olsson et al. (2017).

The interaction between storm movement and catchment response have been studied for a long time. A rainstorm moving in the same direction as the surface flow can amplify the runoff peak (e.g. Yen & Chow 1969, Niemczynowicz 1984, de Lima & Singh 2002). This phenomenon is sometimes referred to as a resonance effect which has its maximum influence when the storm speed equals the flow speed (Ngirane-Katashaya & Wheater 1985; Singh 1997). The temporal distribution of rainfall intensity within a rain event have also shown to influence the catchment response. Temporal variability of rainfall generally results in greater peak discharge compared to constant rainfall (Singh, 1997).

The effect of temporal variability of rainfall as well as storm movement on catchment response has been assessed in previous research. Although previous research have shown the different effects, it is less known how the effect of temporal rainfall distribution relates to the effect of storm movement on urban flood modelling. Furthermore, pluvial flood consequences are not usually within the scope of the studies. The purpose of this study is to fill that gap, aiming at increasing the knowledge of the importance of storm movement in relation to the temporal storm pattern in urban pluvial flooding.

1.1 AIM AND OBJECTIVES

The aim of the thesis is to quantify the relative importance of temporal rainfall distribution and storm movement in terms of urban pluvial flood extent. A hydraulic model of an urban catchment will be forced by different rain scenarios and the objective is to examine the critical parameters associated with pluvial flooding. A second objective is to investigate the flooding results when a CDS-rain and the empirical hyetographs are used as model input. The study aims to address the following questions.

- Is storm movement as critical as the temporal distribution of rainfall when evaluating urban pluvial flooding in terms of maximum flood depth?
- How do the maximum flood depths produced by the empirical hyetographs differ from the ones produced by the CDS-rain?

1.2 DELIMITATIONS

This study will only use a hydraulic model of one urban site. The model will not be calibrated nor validated due to a lack of observations. Furthermore, only rain events with a return period of 100 years will be considered.

2 BACKGROUND

2.1 URBAN HYDROLOGY AND FLOODS

Extreme weather events are usually the forcing of floods and the resulting inundations are categorized based on different characteristics. Fluvial and pluvial floods are two types that are highly relevant for urban areas (Jha et al., 2012). Fluvial floods occur when the water level in watercourses rises to an extent where the bank is overflowed. A fluvial flood can progress slowly due to rainfall with long duration, or fast as a result of cloudburst. This type of flood is the most common in Sweden, where the extreme flows of water derives from intense perception or large quantities of snowmelt (SMHI, 2017). A flood event is called pluvial when the cause is directly from the runoff. This occurs when precipitation or snowmelt cannot infiltrate in the ground or be collected by the drainage system (Jha et al., 2012). The phenomenon is usually related to intense rainfall over a short time period which typically occurs during the summer when meteorological conditions for convective clouds are favorable. July is the month with the most frequent cloudbursts in Sweden (Olsson & Josefsson, 2015).

The runoff generation is a complex hydrological process and is affected by the urbanization of the catchment. The runoff rate will then increase due to more impervious surfaces and the drainage into the collection system. According to Hernebring & Mårtensson (2013), somewhere between 80% and 90% of the yearly precipitation in dense urban areas will runoff at a high rate, compared to 30–50% in undeveloped areas. Non-urbanized areas will have a more delayed runoff process because of the rougher surfaces and better opportunity for infiltration. There are also other interferences that can increase the runoff quantity, such as deforestation and surface compaction (Akan & Houghtalen, 2003). The disturbance of the natural water balance can also lead to a decline in the ground water level (Hernebring & Mårtensson, 2013).

Stormwater drainage systems are an important part of urban infrastructure since they are designed to keep runoff from accumulating on street pavements. The system is a network

of pipes and gutters and has a certain maximum capacity before it starts to surcharge. In Sweden, the policy for which return period of rainfall the drainage system should be designed for ranges between 2–10 years, where the latter applies to city centres and business districts (Svenskt Vatten, 2016).

2.2 STORM MOVEMENT AND TEMPORAL VARIABILITY OF RAINFALL

The influence of the spatio-temporal behaviour of a rainstorm on catchment response have been studied for a long time. Yen & Chow (1969) analyzed the effect of moving rainstorms on surface runoff in a laboratory environment. The study showed that a rainstorm moving in the same direction as streamflow can cause an increased runoff rate. The same phenomenon have later been presented in other studies (e.g Niemczynowicz 1984, de Lima & Singh 2002). Singh (1997) provides a comprehensive review focusing on the effect of different rainstorm characteristics on stream flow hydrograph. A rainstorm moving downstream will delay the runoff from the catchment and when the stream flow from upstream arrives, it will coincide with the rain at the outlet causing a rapid peak in the hydrograph (Singh, 1997). de Lima & Singh (2002) showed that the influence of rainfall patterns causes bigger differences in the hydrographs when the storm moves downstream compared to upstream, when comparing storms with equivalant rainfall intensity distribution.

Catchment response is also a function of the storm speed (Volpi et al., 2013). In general, the magnitude of peak response has the largest values when the storm speed is the same as the flow speed (Singh 1997; Ngirane-Katashaya & Wheater 1985). However, Veldhuis et al. (2018) observed that slow moving rainstorms were associated with higher flows compared to faster moving clouds. The sensitivity to direction and speed is largest when the rainstorm partially covers the catchment area (Surkan, 1974). Seo et al. (2012) used a mathematical approach for studying the influence of storm speed on catchment response for rainstorms with a downstream movement. By introducing a generalized theoretical catchment and describing the rainstorm with different timescales and length scales, the authors extends the relationship between a stationary rainstorm and peak discharge response to now include a moving rainstorm. The authors showed, using the theoretical framework, that a moving rainstorm generates greater flood peaks compared to a stationary rainstorm. The finding is a result of a resonance effect which occurs when the rainstorm moves over the subcatchments. The storm movement shifts the subcatchment's hydrographs and they end up in superposition when the storm speed equals surface flow speed.

The temporal distribution of rainfall have also been found to influence the catchment response. A variability in rainfall intensity generally results in higher runoff peaks compared to constant rainfall (Singh, 1997). Different rain patterns have been used as input in hydraulic modelling with the purpose of investigating the effect on the flood extent (Alfieri et al. 2008; Šraj et al. 2010; Bezak et al. 2018). In all cases, the findings show that rainfall time distribution influence the response of the studied hydrological phenomenon. Mazurkiewicz & Skotnicki (2018b) investigated the effect of different temporal storm distributions on runoff from three urban catchments, focusing on rainfall duration and maximum peak location. The duration of the studied rain events ranged between 15–180

minutes. The simulations showed that longer rains resulted in greater peak discharge compared to shorter rains, which could be explained by the surface retention. The same study also indicates that outflow from the catchments is a function of maximum peak location, where the outflow increases with a later arrival of the peak.

The relative importance of rainfall distribution and total rainfall depth on flood peaks was investigated in a recent study by Hettiarachchi et al. (2018). The authors used a hydraulic model of an urban catchment and simulated five different temporal rainfall patterns. The resulting flood depth varied with more than one meter at one reference point due to the impact of different temporal storm patterns. A variability of similar magnitude was found when the authors considered the different total rainfall volumes. These findings lead to the conclusion that both the temporal pattern of a rain event, as well as the total rainfall depth, are important parameters to consider in hydraulic modelling.

2.3 DESIGN STORMS

A design storm is a rain event with a defined total depth and rainfall intensity distribution that is used in the design process of different hydrological systems (Chow et al., 1988). When simulating floods in hydraulic modelling, a rainfall input needs to be specified and that input is oftentimes a design storm (Prodanovic & Simonovic, 2004). A common way to represent a rain event is to use a hyetograph, which illustrates the time distribution of the rainfall intensities (Svenskt Vatten, 2011). There are many methods for generating design storms, they can be constructed directly from observed precipitation data or by using a synthetically methodology. This section describes two widely used methods for generating synthetic rainstorms.

2.3.1 Intensity-duration-frequency curve

Methods for generating synthetic design storms in stormwater drainage system design and flood estimation are often based on the intensity-duration-frequency (IDF) curve (Svenskt Vatten 2011; Sivapalan & Blöschl 1998). Such curve is a mathematical formulation of the relationship between mean rainfall intensity and rainfall duration for a given return period. The return period of a rain event is defined as the number of years on average between two consecutive events (Chow et al., 1988). One approach is simply to use a design storm with a constant rainfall intensity derived from the IDF-curve based on intended rain duration and return period.

The IDF-curves are based on maximum mean intensities of historical rain events, referred to as block rains. A block rain is defined as the largest mean value of rainfall intensity over a certain time window (duration) of an individually rain event, see Figure 1.

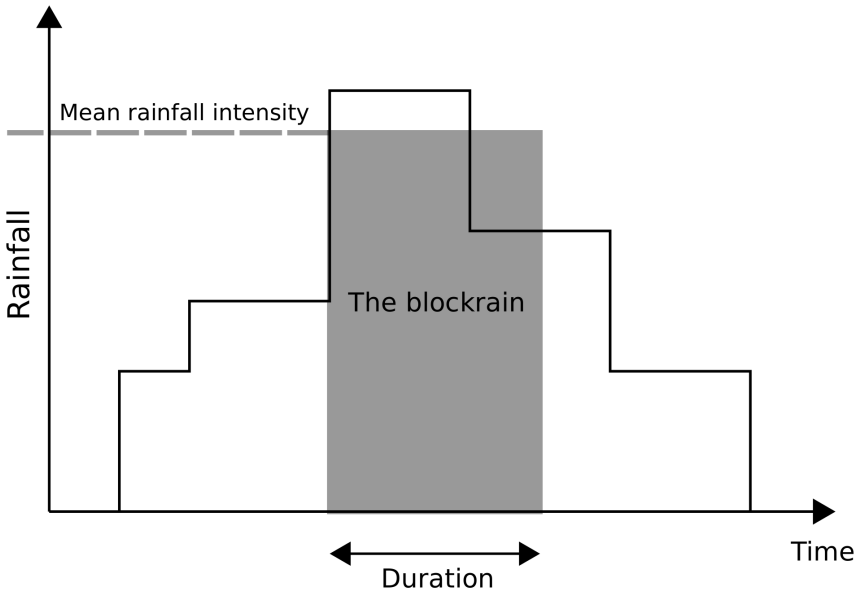

Figure 1. Illustration of a blockrain, which corresponds to the maximum mean intensity for a given duration of a rainfall.

The IDF-curve is constructed by calculating block rains of different duration, and then process each duration separately in a statistical manner. The block rain intensities are ranked in an ascending order and the return period of each intensity value are estimated using a plotting position formula (Koutsoyiannis et al., 1998). The intensities can then be plotted as a function of return period and a probability density function can be fitted to the data points (Svenskt Vatten, 2011). IDF-curves only provide information on the mean intensity for a given duration and return period, hence no information on the time distribution of rainfall intensities can be obtained.

IDF-curves are valid for different geographical areas, which is govern by the rain statistics that has been used in the process. In Sweden, dimensioning rain intensities are recommended to be calculated from the relationship presented in Svenskt Vatten (2011). The equation spells out as

$$i(T_d) = 190 \cdot \sqrt[3]{T_r} \cdot \frac{ln(T_d)}{T_d^{0.98}} + 2 \tag{1}$$

where $i(T_d)$ is rain intensity (l/s·ha), T_d is rainfall duration (min) and T_r is the return period expressed in months. The rain intensity can be converted to mm/h by multiplying with a factor of 0.36.

2.3.2 The Chicago Method

A widely used method for generating design storms is the so-called Chicago method (Prodanovic & Simonovic, 2004). The method, presented by Keifer & Chu (1957), aimed to aid stormwater system development in generating design storms. It consists of two equations, based on an analytic expression of the IDF-curve, that describe the time distribution of rainfall intensities before and after the intensity maximum (da Silveira, 2016). A typi-

cal IDF equation is expressed as

$$i = \frac{a}{T_d + b} \tag{2}$$

where i is the rainfall intensity, T_d is the duration of the rainfall and a and b are non-negative coefficients representing local rainfall conditions. A Chicago-storm can be constructed by first expressing the total rainfall depth (V_d) as

$$V_d = i \cdot T_d \tag{3}$$

Then, by taking the derivative of Equation 3 with respect to the duration

$$\frac{d}{dT_d} V_d = \frac{a \cdot T_d}{(T_d + b)^2} = \bar{i} \tag{4}$$

an expression that describes the rainfall intensity as a function of time ($\bar{i}$) is obtained. Equation 4 has its maximum at time zero. In the Chicago method, Equation 4 is modified and used to describe the rainfall intensities after the peak, and another reversed equation for intensities before the peak. The location of the peak can therefore be placed arbitrary. This is done by substituting the time variable T_d in Equation 4 with

$$\frac{T_d}{r} \tag{5}$$

for intensities before the peak, and with

$$\frac{T_d}{(1 - r)} \tag{6}$$

for intensities after the peak, where r is a factor between 0 and 1 that determines the location of the peak. This methodology enables the peak to be placed arbitrary and the volume will always be correct with respect to the IDF-relationship (Svenskt Vatten 2011; da Silveira 2016).

Chicago design storms (CDS-rains) adapted for Swedish conditions can be calculated as

$$i_{before} = \frac{a \cdot b}{(\frac{|t - rT_d|}{r} + b)^2} + c \tag{7}$$

for intensities before the peak, and as

$$i_{after} = \frac{a \cdot b}{(\frac{|t - rT_d|}{1 - r} + b)^2} + c \tag{8}$$

for intensities after the peak (Svenskt Vatten, 2011). The parameter t denotes time, and a, b and c are tabulated constants that vary depending on the return period. Figure 2 illustrates the resulting CDS-rain when equation 7 and 8 are used for a two hour long rain event with a return period of ten years. The peak is placed in the middle of the event, which corresponds to r = 0.5 and values for the constants are obtained from Figure 1.16 in Svenskt Vatten (2011).

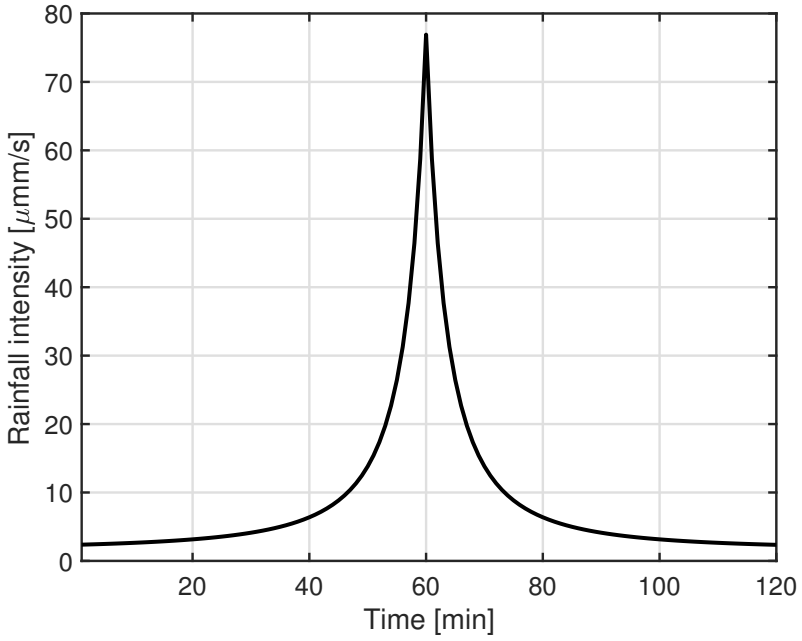

Figure 2. A hyetograph of a Chicago Design Storm (CDS-rain).

A symmetric CDS-rain has a sharpness to it that typically does not resemble real storm events (Svenskt Vatten, 2011). Also, a CDS-rain contains all intensity maximum for every duration, which has been criticized for not reflecting real rain events (Watt & Marsalek, 2013).

2.4 EMPIRICAL HYETOGRAPHS

Olsson et al. (2017) recently investigated the temporal distribution of rainfall intensity in heavy rain events in Sweden. The authors generated five different empirical hyetographs for short ($\leq$ 60 min), medium (60–90 min) and long ($\geq$ 90 min) rain events. A K-means cluster analysis on historical data from rain gauges was used to generate the shapes. The concept of the method is to categorize the events based on their temporal distribution into a predefined number of groups (MacKay, 2002). This was done for every duration class using five groups, hence the generation of the same number of empirical hyetographs. The criteria for a rain event to be included in the cluster analysis was that the average intensity was at least 0.1 mm/min. The rain events were normalized with both duration and total rainfall depth, resulting in dimensionless hyetographs. Therefore, the time axis ranges from 0 to 1 and the total volume adds up to 1. The time series for each event were sampled in 100 points along the time axis, resulting in the same number of intensity values. Figure 3 shows one of the five empirical hyetographs for the long rains.

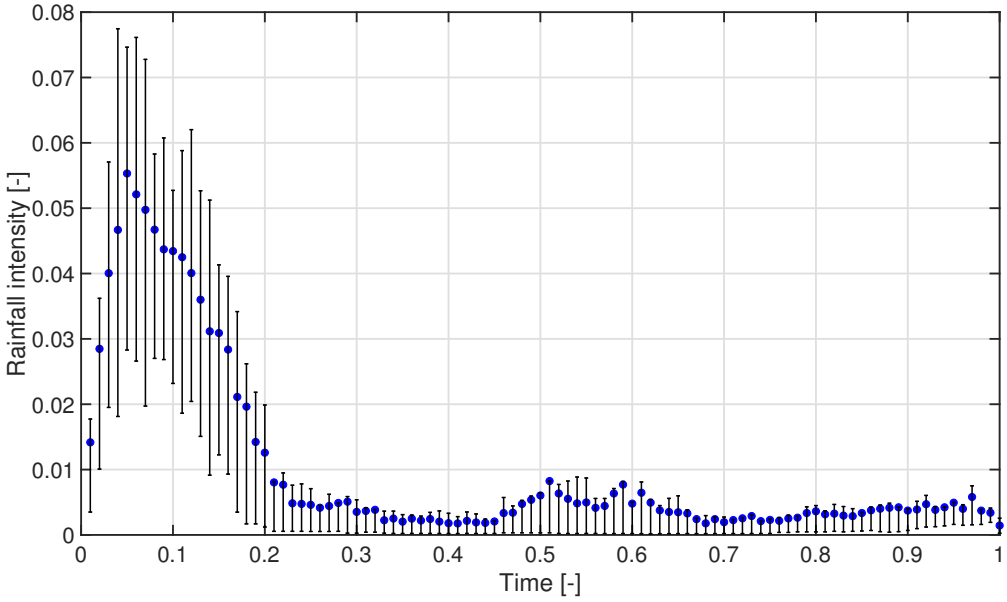

Figure 3. Dimensionless hyetograph based on one of the empirical rain hyetographs developed by Olsson et al. (2017) for storm events longer than 90 minutes. Blue dot represents mean value and the whiskers mark the 25th and 75th percentile.

Large variations in intensity values can be observed in Figure 3, especially the intensities associated with the peak. Since the hyetographs are normalized, rainfall intensities can be obtained by multiplying each data point with a desired rainfall depth. Note that this is only valid if the average intensity for each time step is used, i.e the blue dots in Figure 3. When Olsson et al. (2017) analyzed which empirical hyetographs that best reflect heavy rainfall events, it turned out that there is a tendency for the peak to be located in the first half of the duration.

2.5 URBAN FLOOD MODELLING TECHNIQUES

There are several approaches for modelling pluvial floods in urban catchments. What unites them is the need for high resolution models to accurately simulate the pluvial process (Hernebring & Mårtensson, 2013). The urban landscape is a complex system of artificial structures which divert the flow in irregular ways. Recent advancements in technology have accelerated the number of approaches, which now ranges from simple GIS (Geographic Information System) analysis to coupling of one dimensional (1D) and two dimensional (2D) models. Aspects such as the aim of the simulation, data availability and time frame are important when choosing the most suitable approach. Hernebring & Mårtensson (2013) describe different techniques for modelling pluvial floods, which are summarized in the remaining of this chapter. The techniques are listed based on their complexity.

Surface depression analysis

A GIS analysis can be used for identifying depressions in the terrain. The method is based on a digital elevation model (DEM) and the analysis result will indicate where excess rain

most likely will accumulate. This approach have low requirements on the number of inputs which makes it suitable for a quick overview in flood risk assessment. A common key assumption is that no infiltration occurs which may lead to an overestimation of water volumes.

Modelling of 2D surface flow
This approach computes free surface flow in two dimensions by dividing an area into grid cells and numerically solving the governing differential equation system. In addition to mapping inundated areas, this approach also gives information on water depth, flow directions and flow velocities. Preprocessing of the topographical data is usually needed and the accuracy is strongly dependent on this data, as well as on the grid resolution. A stormwater drainage system cannot be implemented using this technique, although this is usually assessed by subtracting the capacity in the drainage network from the rainfall.

1D-1D modelling of drainage network and street pavements
A method for capturing the dynamics of water flow on surface paths and in the collection system is to couple one dimensional models of the two processes. With this modelling approach, the water in a pipe or a channel can only flow in one direction. Water is exchanged through links between the models which typically are representations of manholes. This approach takes the capacity of the drainage system into account, but is limited to only handle surface flows in predefined directions. The model set-up requires a lot of data and the post processing of the results is time demanding. Mark et al. (2004) investigated the potential and limitations of this approach and concluded that it is best applied for large scale analysis.

1D-2D modelling of drainage network and surface flow
A more accurate way of modelling the dynamics in urban floods, compared to the methods mentioned above, is to couple a 2D model of the urban terrain with a 1D model of the drainage network. This method allows for analysis of both the stormwater drainage system and the flood propagation. Both topographic data and network data are required as input and the 2D part of the computations results in long simulation runs. The accuracy is mainly dependent on the resolution of the 2D model and the way it is coupled with the 1D model.

3 MATERIALS AND METHODS
The analysis of the influence of temporal storm patterns and storm movement on urban pluvial flooding was conducted as a case study. An already developed 1D-2D model of an urban Swedish site was provided and then adjusted to better fit the purpose of the study. The decision on the modelling technique was based on that a coupled 1D-2D model has a good ability to capture flood dynamics since it considers both the terrain and the stormwater drainage system. The following section begins with a description of how the rainstorms, i.e. the hyetographs, were generated. A brief introduction of the modelling software will then be presented, followed by a description of the model setup and adjustments. The implementation of storm movement and the analysis of flow directions in the study area will also be explained. Lastly are the different rainstorm scenarios and the evaluation of the model result presented.

3.1 GENERATION OF HYETOGRAPHS

The empirical hyetographs developed by Olsson et al. (2017) was chosen to represent the simulated rain events in this study, a decision that was based on mainly two reasons. Firstly, they were found to better represent a real storm event compared to other design storms and secondly, the distributions differ in terms of overall shape and location of the peak. The latter made it possible to investigate the influence of different temporal distributions of rainfall, and also relate it to the effect from the storm movement.

The length of the simulated rain events was set to 120 minutes. A few hours are usually applied when studying surface runoff in urban environments (MSB, 2017). The hyetographs that Olsson et al. (2017) generated for long rains ($\geq$90 min) was therefore used. The rainfall depth in the simulations corresponded to a rain event with a return period of 100 years. The reason for this decision was that rainfalls of this magnitude often results in significant flooding (Hernebring & Mårtensson, 2013). The average intensity of the 120 minute long rain was calculated to 32.6 mm/h with Equation 1, which corresponds to a total depth of 65.2 mm. The total depth was multiplied with the dimensionless hyetographs resulting in a rainfall depth for each time step. The hyetographs consists of 100 time steps which translates to 1.2 minutes between each step if a duration of 120 minutes is applied. For clarity, this resulted in 100 blocks of rain each 1.2 minutes long. The total rainfall depth was kept constant in all scenarios not to bias the results.

A CDS-rain is a commonly used design storm in Swedish drainage system design, as discussed in Section 2.3, and MSB (2017) states that it also is a suitable approach in flood hazard mapping. Since a CDS-rain is more or less the standard design storm in Sweden, it was decided to include one in the simulations. By doing so, it was possible to investigate if the flooding extent differs between a CDS-rain and the empirical hyetographs. The CDS-rain was constructed by using a simple application provided by Tyréns. The software uses Equation 1 to compute a hyetograph based on a desired return period, location of the peak and duration. As with the other hyetographs, a return period of 100 years and a duration of 120 minutes were chosen in order to be comparable. Since the total rainfall depth is based on Equation 1 for all hyetographs, the volume was consistent in all scenarios. The peak of the CDS-rain were placed at 37% of the duration, which is a common design practice. A value value between 32% and 48% is recommended by Svenskt Vatten (2011). The intensity values are usually divided into five minute blocks, hence the same was used for the CDS-rain for this study. Note that this differs from the empirical hyetographs which has blocks of 1.2 minutes.

Figure 4 shows the hyetographs with the intensity and time values that were used in the simulations. Each hyetograph has a number associated with it which is used to refer to the different hyetographs from here on. Hyetograph number 1–5 are based on the empirical rain shapes from Olsson et al. (2017) and are ranked based on the location of the peak, the earlier the peak the lower the number.

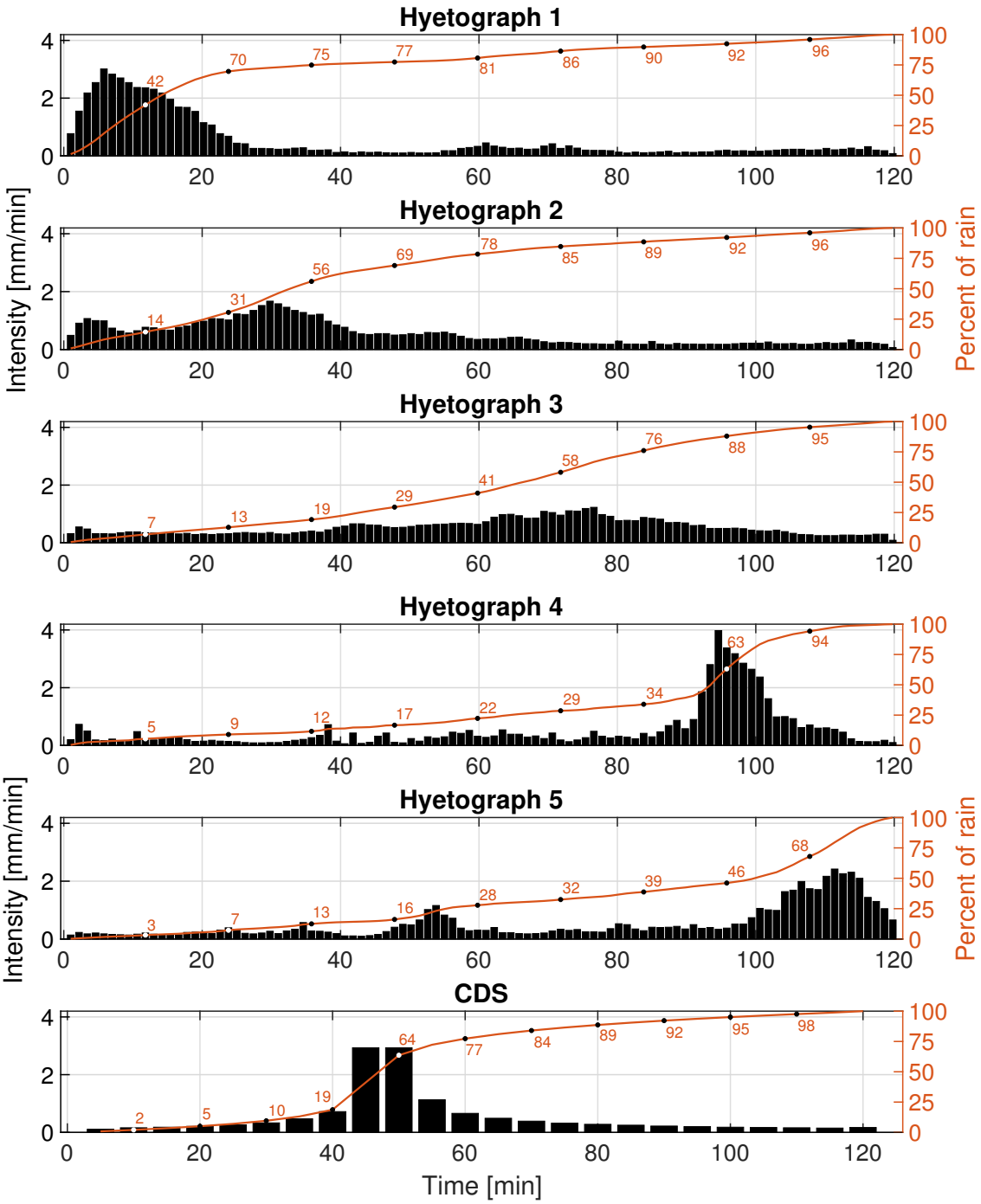

Figure 4. The hyetographs that were used in the simulations.

3.2 1D-2D MODELLING IN MIKE FLOOD

MIKE FLOOD is a software developed by DHI that features hydrodynamic modelling of overland flow and flow in channel and pipe networks (DHI, 2017a). The software allows coupling of the one dimensional modelling tool MIKE URBAN with the two dimensional modelling tool MIKE 21. In this study, a MIKE URBAN model of an urban collection system has been coupled with a MIKE 21 surface model. This section provides an introduction of the used modelling tools.

3.2.1 1D modelling of urban drainage systems

MIKE URBAN is a modelling tool for urban collection and distribution systems (DHI, 2017c). The tool can be run with two different engines, either with MOUSE or SWMM5. The MOUSE engine is developed in house by DHI, while SWMM5 is developed by the United States Environmental Protection Agency (US EPA, 2018). The MOUSE engine has been used in this study, hence no further information on SWMM5 is provided.

MOUSE computes the water flow in the modelled network system (DHI, 2017d). The model simulates unsteady flow under free surface or pressurized conditions. The calculations are based on the Saint Venant's equations for free surface flow, which are derived from conservation of momentum and mass in one dimension. The equations are based on several assumptions such as constant density of the water (incompressible), a small bottom slope and a sub critical flow (DHI, 2017d). A numerical algorithm with finite differences is implemented for solving the differential equations. The Saint Venant's equations need to be modified in order to be valid for pressurized flow in a closed pip, this is done in MOUSE by generalizing the equations and introducing a fictitious slot above the pipe (DHI, 2017d).

The different water conduits of the physical system are represented as links in MIKE URBAN (DHI, 2017d). A link can represent a stormwater drainage pipe or an open channel such as a gutter or a trench. For every link, water level and discharge are calculated continuously over time. Links are defined with two nodes, which are points representing the link ends or a junction connecting other links. The cross-sectional geometry is constant throughout the link and is assumed to have constant slope and material properties. The slope is defined by the elevation of the upstream and downstream nodes and the friction factor associated with the material is expressed as Manning's number (DHI, 2017d).

Elements that connect links are defined as nodes in MIKE URBAN (DHI, 2017d). Four types of nodes are available: circular manholes, basin nodes, storage nodes and outlets. The manhole node is a vertical cylinder, defined by geometrical parameters associated with the size and outlet shape. Basin nodes are used when representing objects such as reservoirs, basins and natural ponds. When using MIKE URBAN alone for simulating surface flooding, storage nodes can be implemented to control the flooded water. Outlet nodes are used where the links interact with a receiving recipient such as a river or a lake. Depending on flow conditions, an outlet node can have a reversed flow and work as an inlet node (DHI, 2017d).

3.2.2 2D modelling of surface flow

MIKE 21 is a modelling tool that simulates surface flow in two dimensions. Many of its applications relates to coastal and marine processes, but the software can also be used for inland processes such as flood modelling (DHI, n.d.). There are different modules available that can be used with MIKE 21, and a central one for modelling free surface flow is the MIKE 21 Flow Model (DHI, 2017b). As with the computations of flow and water level in MIKE URBAN, the 2D flow module is based on the conservation of mass and momentum. The relevance of different forcing in equation varies depending on the simulated process and some can be excluded from the computations. The Coriolis effect and wind stress are examples of forcing that can be neglected when simulating inland flood (DHI, 2017b). The hydrodynamic module uses a so called double sweep algorithm in the computations, which means that the differential equation system is solved in one dimension at a time, alternating between x- and y-directions (DHI, 2017b).

Boundary conditions must be specified if the modelling domain consists of open boundaries, i.e having a flux entering or leaving the modelled area (DHI, 2017b). This can for example be a river inlet and the conditions are usually specified as the water level or a flow rate. MIKE 21 also handles closed boundaries, which means that there are no exchange of flux at the boundaries. This is done by assigning grid cells at the closed boundary with *True land values*, which then encloses the model domain. The latter approach can lead to problems with artificial induced reversed flow, hence caution must be taken when considering the location of the boundaries (DHI, n.d).

The remaining of this chapter will give a brief introduction of the essential model input and parameters when using MIKE 21 Flow Model.

Bathymetry

One key task when modelling surface flow is to define the topography. This is done in MIKE 21 by specifying the bathymetry, which describes the surface depth when not covered with water (DHI, 2017b). The model domain is represented as a rectangular grid with cells of the same length and width. The selection of grid spacing is a central part in order to obtain accurate simulation results. The resolution should be high enough to represent the variation in the topography that diverts the flow. The resolution should not exceed 4x4 m according to Gustafsson & Mårtensson (2014). In MIKE 21, a high resolute bathymetry might lead to stability issues if it is of a varying character. A series of bumps or holes along the flow path might cause that. The stability of the model is related to the Courant Number (C_R) which is defined as

$$C_R = U_{max}\frac{\Delta t}{\Delta x} \tag{9}$$

where U_{max} is the maximum flow velocity (m/s), Δt is the time step (s) and Δx is the grid spacing (m) (DHI, n.d). The Courant number describes how fast information travels over the grid points and the size of the value is a guiding condition for stability (Chow et al., 1988). MIKE 21 can normally handle values up to 5, but a good thumb rule is to never exceed 1 (DHI, n.d).

Time step
The model stability has to be considered when selecting the time step for the simulations (DHI, 2017b). As seen in Equation 9, the Courant number is a function of the time step. Given a grid size and desired Courant number, a maximum length of the time step (Δt_{max}) can therefore be expressed as

$$\Delta t_{max} = \Delta x \frac{C_R}{U_{max}} \tag{10}$$

where the nomenclature is the same as for Equation 9.

Flooding and drying
Flooding and drying is a set of parameters that defines when a cell is flooded and to be included in the surface flow computations (DHI, 2017b). The functionality is govern by two user-defined parameters, h_{flood} (flooding depth) and h_{dry} (drying depth). The parameters work as a threshold that controls when a cell should be checked for flooding or drying. By definition, the following constraint needs to be fulfilled: $h_{flood} > h_{dry}$. When the water level in a cell is greater than the flooding depth, the cell will be wetted and have a non-zero water depth in the result file. A cell can be flooded by accumulating water from an external source, such as a link or precipitation. Flooding can also occur laterally between neighbouring cells, which is referred to as chain flooding. This phenomenon is present when a dry cell has a bathymetry value lower than the elevation of a wet adjacent cell.

A cell is considered dry as long as the water depth is below the drying depth threshold and not risking to be flooded from adjacent cells (DHI, 2017b). When drying occurs, the cell will be taken out of calculation. This methodology allows for moving boundaries since the equations of motion only will apply to wet cells in every time step. MIKE 21 Flow Model has a minimum water depth, which is defined by an *internal engine parameter*. This parameter is by default set to 0.2 mm which is the lowest water depth a dry cell can have. If the water level falls below this value, the water depth will automatically be restored to the minimum value. This is an important aspect since it can affect the mass balance.

Bed resistance
The bed resistance in MIKE 21 can be described with Manning number or Chezy number (DHI, 2017b). The parameters influence the flow speed and are dependent on the nature of the underlying material (Chow et al., 1988). Parameter values have been derived empirically for a number of different materials. The surface flow computation uses the Chezy factor, so if a Manning number is declared, it will be converted to the corresponding Chezy number (DHI, 2017b).

Infiltration and leakage
There are two approaches for handling infiltration and leakage in the surface zone, *Net infiltration rates* and *Constant infiltration with capacity* (DHI, 2017b). With the first approach, every cell will have a specified infiltration rate that always will be sustained. Water will infiltrate as long as there is enough water to classify the cell as wet or flooded, hence no capacity of an unsaturated zone is considered. Since MIKE 21 does not have a

vertical dimension, the infiltration works as a sink that basically just removes water from a cell. A cell's water depth (H) that follows the infiltration is calculated as

$$H = H_0 - \frac{V_{infiltration}}{A} \tag{11}$$

where H_0 is the water level prior the infiltration (m), $V_{infiltration}$ is the infiltrated volume (m^3) and A is the surface area of the grid cell (m^2) (DHI, 2017b).

The other approach, *Constant infiltration with capacity*, models the dynamic of water flow between the surface and a saturated and unsaturated zone (DHI, 2017b). The unsaturated zone is represented as an infiltration layer which is categorized by its volume and porosity. Porosity is the ratio of the volume of the voids and the total volume in a soil, and is assumed to be constant throughout the infiltration layer. The infiltration is governed by a prescribed flow rate, which remains constant in the simulation. The flow between the unsaturated and saturated zone is referred to as leakage, which is govern by another constant flow rate. When the two dimensional surface flow computations has been proceeded at a time step, the leakage volume ($V_{leakage}$) is calculated for relevant cells as

$$V_{leakage} = Q_l \cdot \Delta t \cdot A \tag{12}$$

where Q_l is the leakage flow rate (m/s), Δt is the time step length (s) and A is the size of the cell (m^2) (DHI, 2017b). If Equation 12 results in a volume that exceeds the water content in the infiltration layer, the total amount of water will leave the layer. The computation of the volume of surface water that infiltrates is analogous with equation 12, but with another flow rate. Also, the algorithm checks if there is enough room in the infiltration layer, since the volume from infiltration cannot exceed the storage capacity in the layer (DHI, 2017b).

3.2.3 Coupling of models

The surface flow model and the drainage network model can be connected in nodes by the use of urban links (DHI, 2017a). An urban link allows for an exchange of water between the two model types and should therefore be located where the two systems interact. Manholes and outlets are natural choices for the use of urban links. The urban link between the surface model and a manhole is called ***M21 to inlet*** and can be connected to one or more grid cells in the MIKE 21 model. The flow through an urban link can be computed with the weir equation which takes different forms depending on if the manhole is submerged or not. If no flooding occurs, the discharge (Q) is calculated as

$$Q = C(H_U - H_{M21})W_{crest}\sqrt{2g|H_U - H_{M21}|} \tag{13}$$

where H_U is the water level in the drainage system (m), H_{M21} is the average water level on the ground (m), W_{crest} is the width of weir crest (m), g is the gravitational constant (m/s^2) and C denotes the discharge coefficient which typically is equal to one (DHI, 2017a). A modified expression of Equation 13 is used if the node is surcharged, which spells out as

$$Q = C(H_U - H_{M21})W_{crest}\sqrt{2g|H_U - H_{M21}|}\left(\frac{|H_U - H_{M21}|}{max(H_{M21}, H_U) - H_g}\right) \tag{14}$$

where H_g is the ground level at the urban link (m) (DHI, 2017a).

A coupled model might encounter stability issues when the water level in the surface model and the pressure head in the drainage network model are similar at an urban link (DHI, 2017a). This issue can be assessed by introducing a parameter called QdH. The parameter works as a threshold value that determines at which water level difference a suppression factor should be activated. The suppression factor downscales the discharge in Equation 14. The suppression factor is dependant on the water level difference (dh) and is calculated by

$$Suppression\ factor = 1 - (\frac{(QdH - dH)}{QdH})^2 \tag{15}$$

If the water difference (dh) is greater than QdH, the suppression factor takes the value 1 (DHI, 2017a).

3.3 IMPLEMENTATION OF STORM MOVEMENT

This section describes how the storm movement was implemented in MIKE 21. The rain cloud was assumed to be of the same geometry as the model domain, i.e. a rectangle, moving parallel with the model grid with full coverage in the lateral direction, see Figure 5.

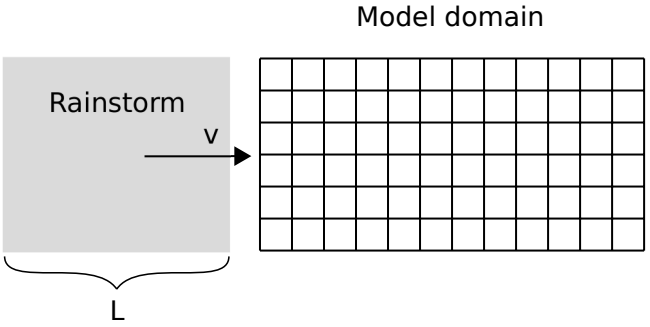

Figure 5. A schematic of how the storm movement was set up.

Both direction and speed was assumed to be constant as the storm advances over the domain. The rain extent of the cloud in the moving direction (L) is therefore defined by the speed (v) and the duration of rain in every grid cell (T_R), expressed by

$$L = v \cdot T_R \tag{16}$$

A literature review was carried out to determine a realistic storm speed to be implemented in the simulations. Moseley et al. (2013) studied convective and stratiform rain cells based on radar data and synoptic cloud observations in Germany by using a tracking algorithm. Convective cells are characterized by a distinct peak in rainfall intensity, implying a tendency to produce a lot of rainfall over a short period of time (Moseley et al., 2013). Stratiform precipitation on the other hand, have a much more uniform distribution of intensities. The authors found that the mean flow speed ranged between around 8 and 12 m/s depending on the precipitation type. Convective cells have speeds in the lower end of the range, while stratiform cells are faster. Convective precipitation is important

from a flood risk point of view. It was therefore decided to use a storm speed of 8 m/s since it seemed to be a representative speed for convective rain cells and that most of the hyetographs that were used for the simulations have a convective characteristics. Willems (2001) developed a stochastic rainfall generator adapted for small spatial scales, which was calibrated against data of a dense network of rain gauges in Antwerp, Belgium. The author derived a Weibull distribution for storm speed probability, which is plotted in an article by Vaes et al. (2002). A speed of 8 m/s is well placed within the range of the most frequent storm speeds. This is also true for the storm speeds that was found by Niemczynowicz (1984), when analyzing 400 rain events in Lund, Sweden. The selected storm speed was therefore considered an adequate choice. The length of the cloud, according to Equation 16, is therefore 57.6 km with a speed of 8 m/s and a rain duration of 120 minutes.

The storm travels a distance of

$$\Delta l_{cloud} = v \cdot \Delta t_{cloud} \tag{17}$$

for a given time increment Δt_{cloud}. For each time increment, the storm covers an additional part of the model domain. Precipitation is then initialized in the newly covered area. Figure 6 shows the discrete movement of the rainstorm over the model domain.

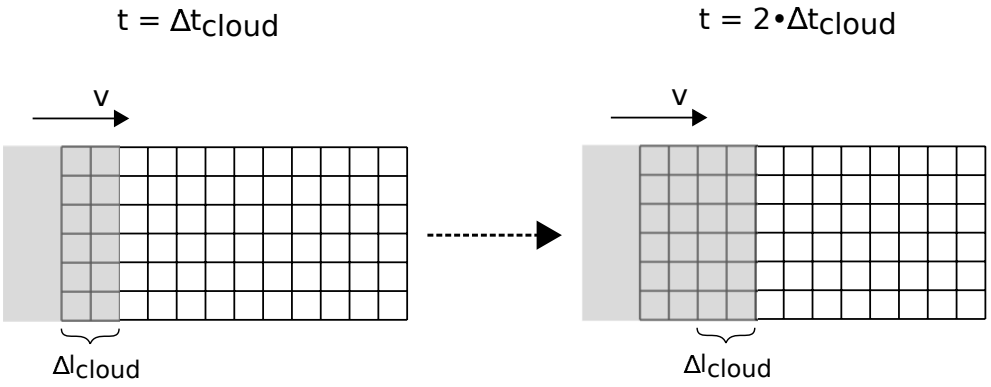

Figure 6. A schematic of how the rainstorm advances over the model domain in two time steps.

Since the surface flow computations are carried out in grid cells, the storm cannot partially cover the grid cells in every time step in order to obtain the correct storm speed. Hence,

$$\frac{\Delta l_{cloud}}{\Delta x} \epsilon \mathbb{Z} \tag{18}$$

must be fulfilled, where Δx denotes the grid size. The time steps in which the storm advance over the domain is therefore a function of grid resolution. This implies that it is not obvious that Δt_{cloud} can be set equal to the time step of the surface flow computations. The model had a resolution of 4x4 m and the cloud time step (Δt_{cloud}) was set to 5 s. This translates to a discrete cloud movement (Δl_{cloud}) of 40 m considering a storm speed of 8 m/s.

When Δt_{cloud} had been decided, the model domain was divided into sub-areas representing the new coverage of the storm for each time increment. A hyetograph was then

mapped to all grid cells within the sub-area. All sub-areas were assigned the same hyetograph but with a time lag depending on the location relative to the axis along the direction of movement. If k denotes the number of time increments, the time lag for each sub-area can be calculated as

$$t_{lag} = \Delta t_{cloud} \cdot (k - 1). \tag{19}$$

Figure 7 illustrates how the model domain was classified into sub-areas and the mapping of the hyetographs.

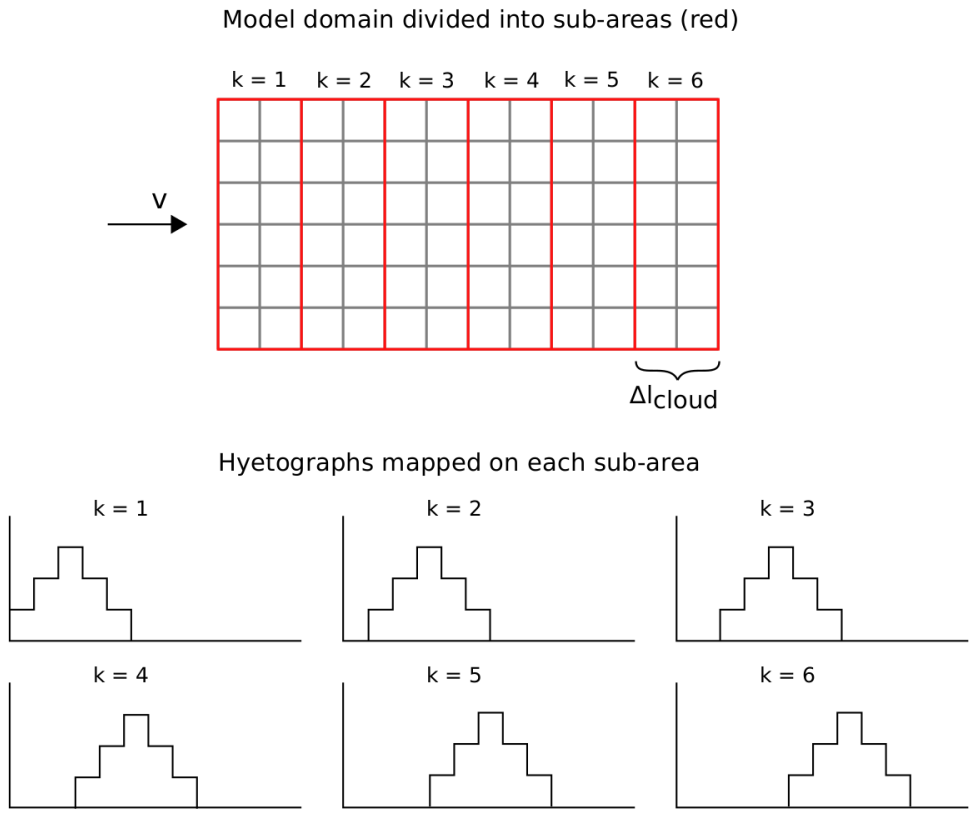

Figure 7. A schematic of how the model domain was divided into sub-areas (red grid) and mapped with corresponding hyetograph.

The implementation of the storm movement was done in MIKE 21 by using the tool *dfs2+dfs0 to dfs2*. The name refers to different file formats developed by DHI for storing data. Gridded data are stored as *dfs2*-files and time-series, such as precipitation data, are saved in the *dfs0*-format. A grid with the same spatial properties as the model domain was created and all grid cells were assigned a unique grid code, associating a cell with its sub-area. The grid code worked as an identifier for which hyetograph (with associated time lag) that should be mapped onto the cell. The time lag was calculated for each sub-area and the hyetographs were created as a time series and saved in the *dfs0*-format. The longest time lag was calculated to 8 minutes. This implies that it will rain for 2 hours and 8 minutes if the model domain is viewed from an Eularian perspective. For clarity,

the prolonged rain duration is only due to the storm movement, each grid cell was still exposed with rain for two hours. When the tool was run it resulted in a series of grids where each cell contained the correct rainfall intensity.

3.4 STUDY AREA

A 1D-2D model of the urban locality Smedby, located in Kalmar municipality, was used for the flood simulations in this study. Smedby has around 3700 inhabitants and is situated close to Sweden's south east coast, less than 10 km west of the city Kalmar (SCB, 2018b). The model domain includes the whole urban area of Smedby and covers about 6 km^2. Figure 8 shows the study area in terms of land use and land cover.

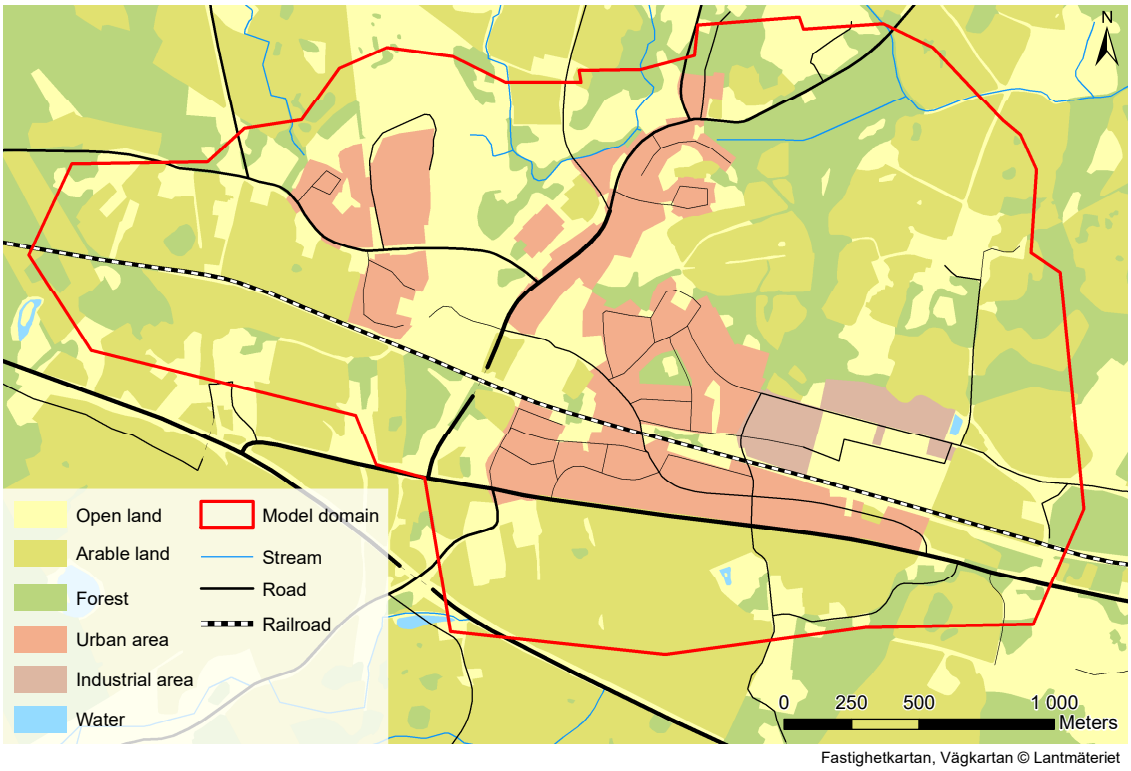

Figure 8. Land use and land cover of Smedby, the study area.

Smedby is characterized by an urbanized center and plenty of arable land close by. There is a railroad intersecting the area and three stream inlets at the north border of the model domain which has its outlets in the north east corner. The urban area is located south of the stream network.

3.5 MODEL SET-UP

3.5.1 MIKE URBAN model of the drainage system

A MIKE URBAN model of the stormwater drainage system in the study area was provided by Kalmar municipality. The model consisted of essential parts of the system such as pipes, manholes, basins and outlets, but the model also had the streams represented. As seen in Figure 8, Smedby has a small stream network in the northern part of the area. The streams had been implemented as open channels with a defined cross sectional shape. These open channels stretch along the whole extent of the streams and therefore contribut-

ing with a flow from the upstream catchment. At locations where a stream is close to the urban development of Smedby, the stream enters a culvert. This occurs at two locations. The incoming streams and the rural catchments associated with them were decided to be excluded in the MIKE URBAN model for this study. This decision was based on mainly two reasons, where one was that the upstream catchments are large, altogether around 12 km^2, which would have been too large to be included in the MIKE 21 terrain model considering the run times it would result in. Also, the streams contribute with a fluvial flow which is not a process that is within the scope of the study. Since the focus of the study was on pluvial processes in an urban environment, the exclusion of the rural catchments and streams was considered a valid choice. Noteworthy is that the part of the stream that is linked between the two culverts were kept in the model, since it enables a connection between the north western and north eastern part of the drainage system.

Before any coupled simulation runs were proceeded with, the performance of the MIKE URBAN model were thoroughly checked. The network was loaded with a runoff input of a 10 year rain and log and result files were studied with respect to unwanted behaviour. A flaw that was discovered early on was that many of the pipe dimensions exceeds the connecting node, the manhole. When the diameter of the pipe is larger than the diameter of the manhole, which has a cylindrical shape, the water is instantaneous forced into a smaller space which might result in irregular flow curves. This inconsistency was true for more than 30% of the nodes. The difference between the dimensions ranged between a few centimeters and, in some rare cases, up to 80 centimeters. This issue was not assessed any further since it would have been too time consuming to manually alter the node dimension to match the connected pipes. The bias from this issue was considered negligible in terms of flooding consequences since the runoff from the simulated rainstorms (100 years) largely exceeds the capacity of the drainage system (10 years). Furthermore, this issue was present in all simulation runs and since the aim was to study relative differences the issue was not considered critical enough for the model to be modified.

A pipe with a negative slope can indicate an incorrect implementation. The cause is usually that the nodes that represent the start and the end of the pipe are mixed up, which makes the calculation of the slope false. A negative slope does not necessarily mean that this is the case though, since the real drainage system might have sections with negative slopes. To assess this possible error, all pipes with a negative slope were checked with respect to the start and end node. If the nodes were mixed up, which were true in some cases, they were corrected.

MIKE URBAN generates a summary file with every simulation run containing information on the computational performance. It includes a mass balance calculation which can provide an indication of the model robustness. The mass balance results were checked for each simulation run and will be presented and discussed later on in this report.

3.5.2 MIKE 21 model of the terrain

A MIKE 21 model of the study area, developed by Tyréns, was used for the simulations in this study. This section describes the set-up and the adjustments of the model that were performed.

Bathymetry

The bathymetry has a resolution of 4 m and the model domain had been enclosed by grid cells with *True land values*. Cells with a *True land value* stays inactive throughout the simulation, hence no water exchange occurs over the boundary. This implies that the water in the MIKE 21 model can only leave the surface either if it infiltrates or reaches a manhole and enters the MIKE URBAN model. It was decided to proceed with the original extent of the model domain since the distance between the boundary and the urbanized part of the study area was considered substantial enough. The bathymetry of the model domain is illustrated in Figure 9. Note that the elevation is only shown for active cells in the model domain.

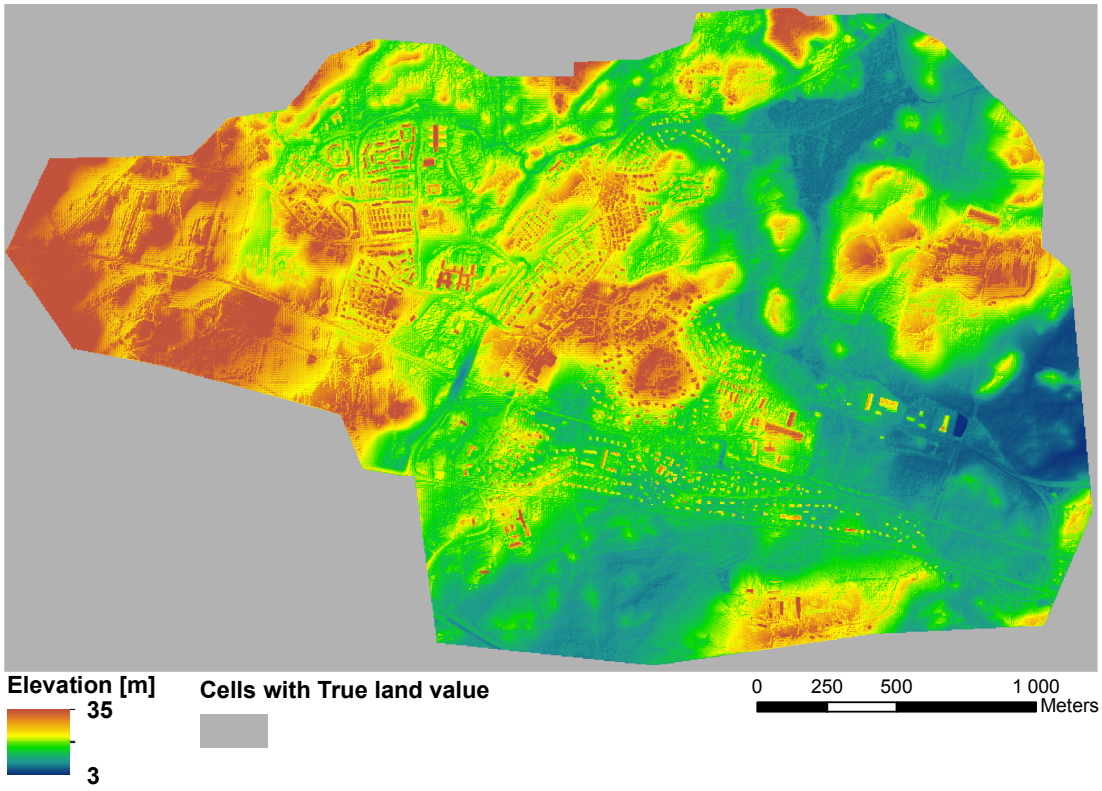

Figure 9. The bathymetry, i.e the topography, of the model domain. All grid cells in the grey are have been assigned *True land values*, meaning that they are excluded from the flood computations and thus so make up a closed boundary.

The bathymetry file had been reconditioned on beforehand with respect to the buildings in the area. The original DEM, which the bathymetry is based upon, did not contain the elevation of the buildings. The buildings had therefore been elevated to better represent the real flow paths and to avoid the risk of water flowing over them. The bathymetry file was checked for if bridges and tunnels were represented in a correct way. This was carried out by comparing the bathymetry with aerial photos of the area. If the elevation at the location of the structures is not lowered, the water that flows beneath will be embanked (MSB, 2017). The surface under the bridge had been lowered on before hand, but

four smaller culverts were found that had to be adjusted for. The method for lowering the culverts was to delete the elevation at the location of the culvert and then interpolate between grid cells on each side.

Time step
The time step was set to 0.2 seconds in all simulations. The value was considered small enough to reduce the impact of instabilities and still resulting in reasonable run times. Also, the Courant number associated with each simulation was evaluated and did never exceed 1. In fact, it ranged between 0.05–0.1 and was therefore below the critical value of 1 with a great margin. Longer time steps were tested but those simulation runs suffered from a few local instabilities, hence the choice of 0.2 seconds.

Flooding and drying
The flooding and drying depth was set to 8 mm and 3 mm, respectively. The values are within the range of recommended values by DHI, which are 2–50 mm for the flooding depth and 1–20 mm for the drying depth (DHI, 2017b). In general, smaller values reduce the risk for mass balance errors which was why parameter values in the lower end were used.

Bed resistance
A grid file with two different Manning's values were used. Hard surfaces such as rooftops, roads and parking lots were assigned a value of 50 $m^{1/3}/s$. For all other land cover, 2 $m^{1/3}/s$ was used. These values are a good representation of the bed resistance of overgrown and hardened surfaces (Gustafsson & Mårtensson, 2014). Figure A.1 illustrates the spatial distribution of the values in the model domain.

Infiltration and leakage
Constant infiltration with capacity was the technique that was used for handling the dynamics of infiltration. As discussed in Section 3.2.2, parameters that define the volume and infiltration flow rates had to be defined. A grid file containing values for these parameters had been prepared by Tyréns on before hand. The porosity and the infiltration and leakage rates are based on the soil types in the area. A low initial water content was set since the occurrence of cloudburst in Sweden are concentrated to the late summer months (Olsson et al., 2017) when soil moisture is assumed to be low. The parameter values are summarized in Table 1. The reader is referred to Figure A.1 for maps of how the values are distributed.

Table 1. Parameter values associated with the infiltration in the model. The areas within the model domain that were assigned the different values are also tabulated. Q_i and Q_l denotes the infiltration and leakage rate, respectively.

Parameter	Value	Assigned to
Q_i [mm/h]	36.000	Non hardened surfaces
	0.001	Impervious surfaces
Q_l [mm/h]	180.00	Granular soil
	0.40	Silt and clay
	0.36	Till
	0.01	Non hardened surfaces
Porosity [-]	0.40	Non hardened surfaces
	0.01	Impervious surfaces
Initial water content [% of capacity]	20	The whole study area
Depth [m]	0.30	Non hardened surfaces
	0.01	Impervious surfaces

Mass balance
As with MIKE URBAN simulations, MIKE 21 also produces a summary file with a mass balance calculation which indicates the model's computational performance. The mass balance were checked for every simulation and will be presented and discussed further on in the report.

3.5.3 Coupling parameters

The MIKE 21 and MIKE URBAN model were coupled via the manholes through urban links. The coupling took place between the manhole and one overlapping grid cell in the 2D model. No outlets in the MIKE URBAN model were coupled since the discharge at the outlets were considered to not affect the flooding situation in the urban area. All connected nodes were thoroughly checked so that no grid cell were coupled with more than one manhole. Such situation can result in model instabilities and volume errors (DHI, 2016). Two coupling nodes were found having this issue and was resolved by coupling the manholes to separate, neighbouring cells.

The weir equation (Equation 13) was used for the computations of the water exchange between the models. The crest width was set to 3.14 m which corresponds to a manhole circumference of 1 m and a max discharge of 0.3 m^3/s was set for all coupling nodes. The initial simulations suffered from oscillating flows in some of the coupled node. A QdH factor of 5 cm was therefore set which resolved the problem, see Section 3.2.3 how the factor suppresses the flow between the models. A few other QdH values were tested, both larger and smaller, but they all generated similar results.

3.5.4 Directions of storm movement

The study area had to be analyzed in terms of dominating flow direction. As discussed in Section 1, a storm moving in the same direction as the flow might cause a resonance effect leading to higher runoff peaks. The objective was therefore to find the dominating

flow direction and simulate a rainstorm that moves parallel to it. In order to properly investigate the influence of the movement, reference scenarios where the rainstorm moves against and perpendicular to the flow direction were intended to be implemented. There are two properties that govern the surface flow in the 1D-2D model, namely the topography in the terrain model and the drainage system in the MIKE URBAN model. Surface runoff will be controlled by the topography until some part of it reaches a manhole where it will be diverted to the stormwater drainage system. It was therefore necessary to study the flow direction both in the drainage system and on the surface.

An analysis of the surface flow direction was conducted in ArcGIS. Note that this part only considered the terrain and not including the stormwater drainage system. The tools that were used for the analysis is part of the Arc Hydro Tools which is a toolbox developed for water resource applications (ESRI, 2011). The DEM-file (Digital elevation model) was first reconditioned with the tool *Fill Sinks*. A sink is a grid cell that has a lower elevation than all adjacent cells and the water will accumulate in that cell and not be able to flow further. To eliminate this problem, *Fill Sinks* changes the elevation value to match the surrounding elevation cells. The flow direction for each grid cell was then calculated with the tool *Flow Direction*. The tool outputs a raster where each grid cell has a value that indicates the flow direction for that particular cell. The flow direction is governed by the elevation of the surrounding grid cells and is determined by the direction of the steepest drop. Data of the direction of where the water flows towards in each grid cell had now been obtained and was analyzed further. The frequency distribution was studied by creating a histogram of the different directions, see Figure 10.

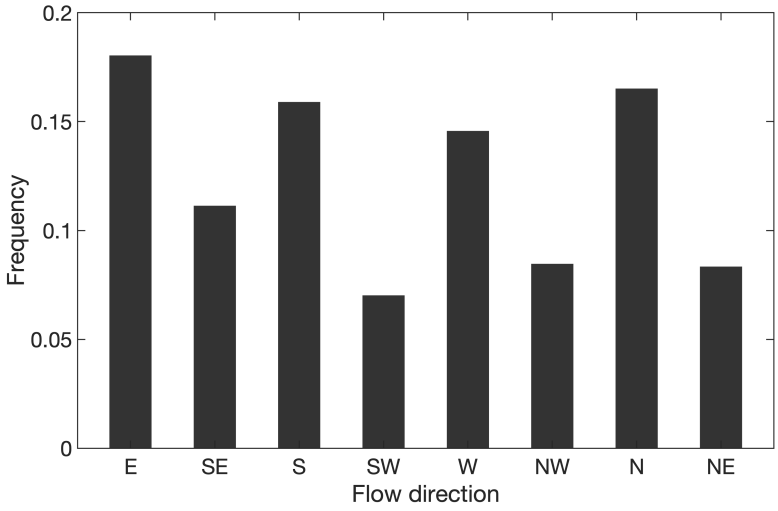

Figure 10. The frequency distribution of the flow directions for all cells in the bathymetry grid. E indicates eastward, SE is southeastward, S is southward, SW is southwestward, W is westward, NW is northwestward, N is northward and NE is northeastward.

East is the most frequent flow direction, but the difference is not large compared to the south and north flow directions. Hence, no dominating flow direction could be determined from the distribution in Figure 10 alone.

An analysis of the spatial distribution in the flow paths was carried out to further investigate the flow characteristics of the study area. By using the raster with flow direction as input, the tool *Flow Acummulation* in ArcGIS counts the the number of upstream cells whose water is flowing to each cell. The output is a grid were each cell contains the number of upstream cells. Based on that output, a network of streams were created with the tool *Stream definition*. The density of the stream network is governed by a threshold value, where a smaller value usually results in a denser network of streams. The threshold value was adjusted so that an adequate number of flow paths were generated, meaning enough flow paths to cover most of the study area. The result from these steps were a network of flow paths which are shown in the top map in Figure 11.

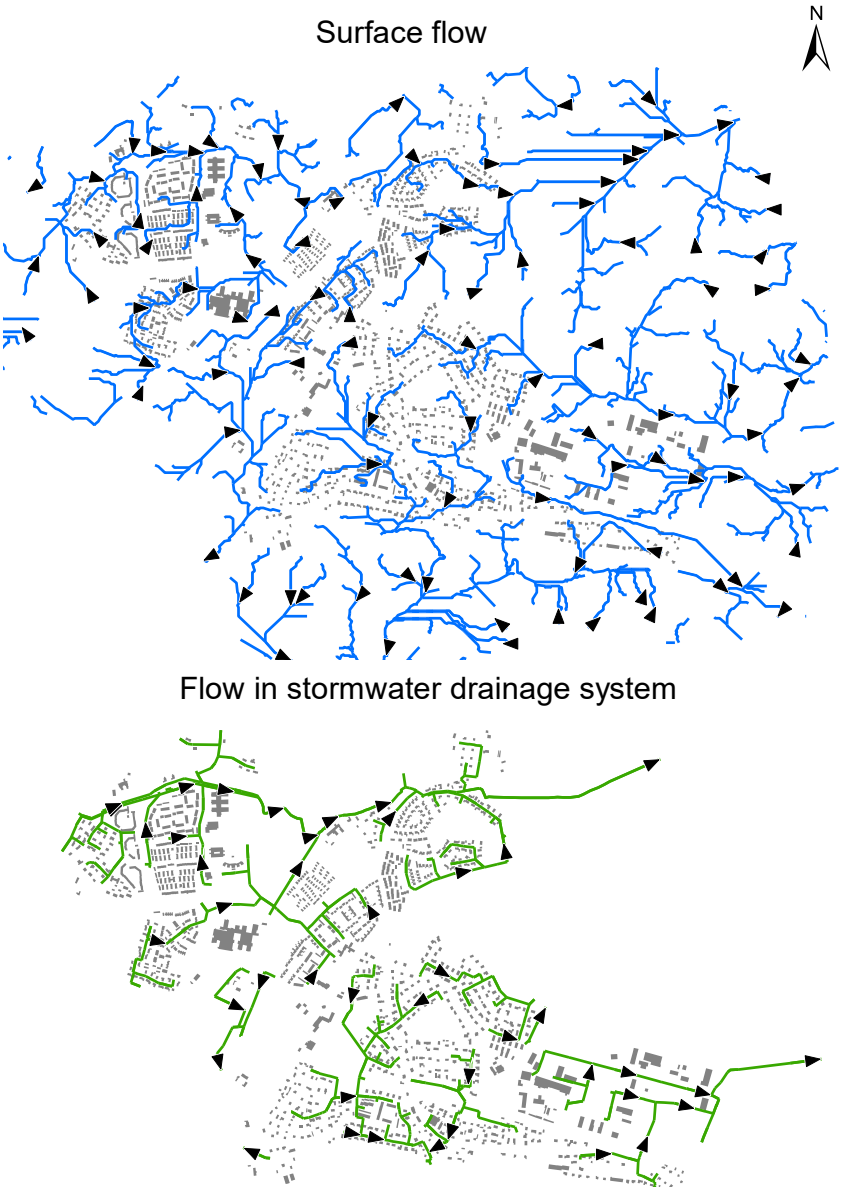

Figure 11. Flow directions based on the topography (upper map) and stormwater drainage system (lower map).

The dominating surface flow direction for the northern part of the model area seemed to be eastern when studying the flow paths in Figure 11. No obvious predominate direction could be found for the rest of the area, although the south eastern part have a rather consistent eastern flow direction. The flow directions in the stormwater drainage system were, to a large extent, considered coherent with the surface flow directions. When studying Figure 11, it was clear that the northern half of the drainage system mostly has an eastern slope. Furthermore, the longest stretch of connected pipes that have a consistent direction is east, which was concluded from the same figure.

The dominating flow direction of the study area was defined as eastern when all of the aspects that are described above were considered. Hence, the directions of the storm movement that were implemented in the model were decided to be east, west and north. The perpendicular direction, north, were arbitrary decided.

3.6 EXPERIMENT SET-UP

Table 2 summarizes the rain input that was used in the simulations. A grid file containing the rainfall from the moving or the stationary rainstorm was created for every scenario, see Section 3.3 for the methodology. The model was then run with the different grid files as rain input. Scenarios with a stationary rainstorm have the direction ”None” in Table 2.

The hyetograph and the direction of movement were the only parameters that were altered between the runs. Since all other parameters were fixed, it was possible to investigate the influence of storm movement and the temporal rainfall distribution. Other rain related parameters, which had the same values in all scenarios, were as follows.

Total rainfall depth: 65.2 mm
Storm speed: 8 m/s
Rainfall duration: 120 min
Simulation duration: 180 min

The rainfall was initiated right at the beginning of the simulations and the flow computations continued for about 1 hour after the rainfall had stopped. The latter made sure that maximum flood depths were reached within the time of the simulation.

Table 2. The different rainstorm scenarios that were carried out in the flood modelling, including the direction of movement and hyetograph.

Scenario	Direction	Hyetograph	
1E	East	1.	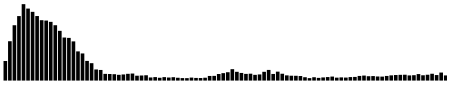
1W	West		
1N	North		
1St	None		
2E	East	2.	
2W	West		
2N	North		
2St	None		
3E	East	3.	
3W	West		
3N	North		
3St	None		
4E	East	4.	
4W	West		
4N	North		
4St	None		
5E	East	5.	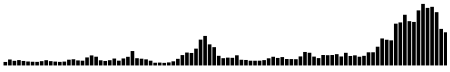
5W	West		
5N	North		
5St	None		
CDSE	East	6.	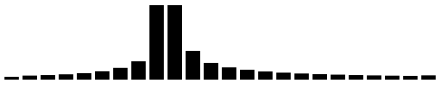
CDSW	West		
CDSN	North		
CDSSt	None		

3.7 EVALUATION POINTS AND PARAMETERS

Maximum flood depth was chosen as the main evaluating parameter when the results from the flood simulations were analyzed. Flood depth is a critical parameter in terms of damaging flood consequences and was therefore considered an important parameter to investigate. The timing of the maximum flood depth was also investigated. The parameters were evaluated at certain locations in the study area. This was a critical part of the methodology since the results of the study would be based on these locations only. The following criteria were set up when the evaluation points were chosen.

- Flooding occurs at the location
- Not close to the border of the model domain
- The evaluation points were to be spatially distributed over the whole model domain
- Mainly downstream and upstream locations
- An adequate amount of points to strengthen the relevance of the results

Ten evaluation points, i.e. grid cells in the 2D model, were picked out based on the criteria above. The majority of the points are located in the northern part of the model

domain, since a consistent eastern flow direction is present there. The locations were also evaluated with respect to model stability by making sure that no abnormal behaviour occurred nearby. Also, the flood depth development over time at all evaluation points were analyzed to assure that the maximum flood depth had been reached within the time frame of the simulation. This was done for all scenarios. Note that the location of the evaluation points were decided before the simulations were further analyzed with respect to the influence of storm movement and temporal variability of rainfall in order to not bias the results of the study. The evaluation points are presented in Figure 12.

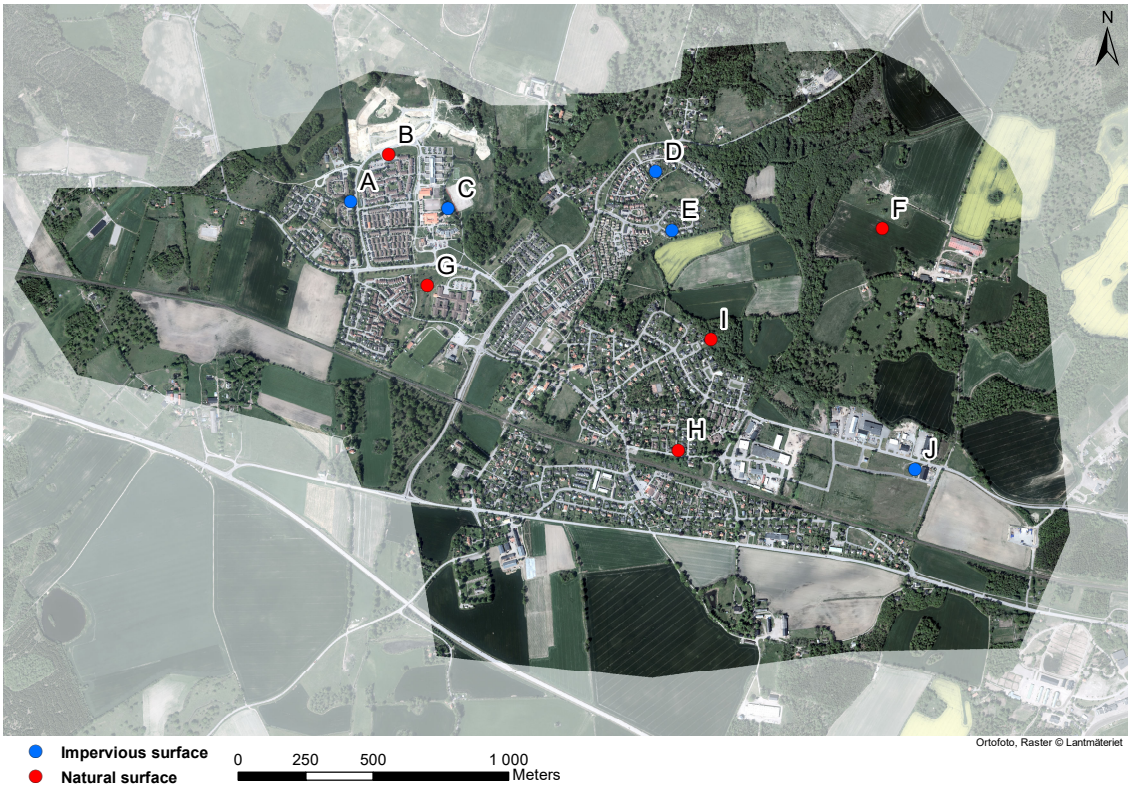

Figure 12. Locations and surface type of the ten evaluation points that were used in the study.

To investigate how well the results at the evaluation points reflect the behaviour at all locations in the study area, a map of the difference in maximum flood depth between the CDS-rain and Hyetograph 3 was created, see Appendix B. Those specific hyetographs were selected based on that they generated the highest and lowest flood depths in the simulations. The choice of evaluation points is further discussed in Section 5.3.

Surface flow speeds were investigated since it is an important parameter in the dynamic between storm movement and catchment response (e.g. Singh 1997). A map of maximum surface flow speeds in the grid cells for Hyetograph 1 in a non-moving scenario was created. In addition, two types of weighted arithmetic means of the flow speed in different areas were calculated. One mean value was based on each grid cell's maximum flow speed, while the other used the average speed over the first hour. Both means were weighted with the cell's average flux density. Definitions and methodology for the statis-

tical calculations are described in Appendix F. The calculated means for the non-moving scenario with Hyetograph 1 are presented in Table C.1.

Maps of the moist content in the soil layer at the time when the peak of Hyetograph 1 and 4 arrives were created. This analysis was conducted since it could help to explain the flood response in terms of the different hyetograph characteristics. The maps are presented in Appendix D and further discussed in Section 5.2.

4 RESULTS

The influence of storm movement and temporal distribution of rainfall on maximum flood depths was investigated by simulating six different hyetographs and three directions of storm movement. An eastern direction of movement will be referred to as the downstream direction, west as the upstream direction and north as the perpendicular direction of movement. The simulation results from ten evaluated locations are presented in the following chapter, starting with the effect from storm movement, followed by the influence of different hyetograph and lastly a comparison between the flood depths from the empirical hyetographs and the CDS-rain. Data on the maximum flood depths in all scenarios can be found in Appendix F.

4.1 THE EFFECT OF STORM MOVEMENT

4.1.1 Time arrival of maximum flood depth

It is intuitive that the direction of movement would effect the timing of the maximum flood depth at the evaluation points. This parameter was therefore investigated to see if it was the case for the simulations in this study. The plots in Figure 13 illustrates how the water level at evaluation point B, F and H evolves over time and also when the maximum flood depth and peak intensity arrives, depending on the rainstorm's direction of movement. The chosen evaluation points make up a triangle covering the greater part of the model domain. Data on the timing of the peak depth in all scenarios is summarized in Table E.1 in Appendix E.

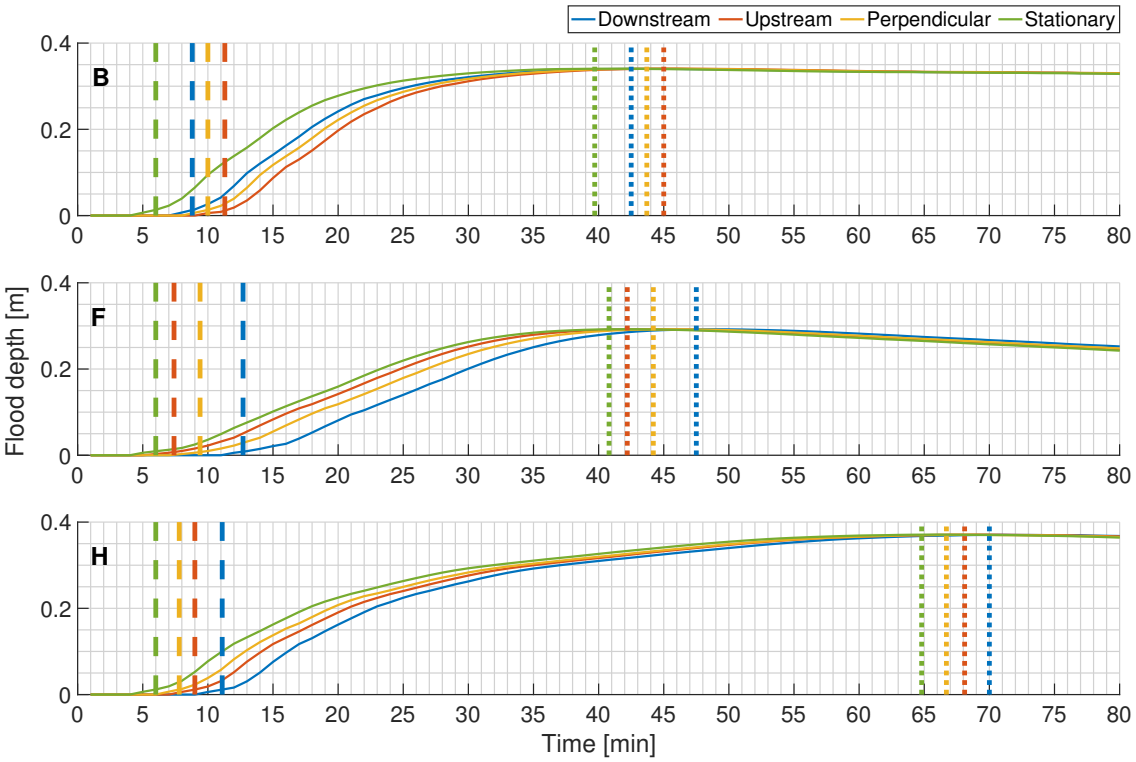

Figure 13. Flood depth as a function of time at evaluation point B, F and H when Hyetograph 1 was used as rain input. Each plot illustrates how the flood depth develops over time depending on the rainstorm's direction of movement. The plot also indicates the timing of the most intense rainfall (dashed line) and the time of when the maximum flood depth occurs (dotted line).

It is clear from Figure 13 that the arrival of the maximum flood depth is a function of storm movement. The earliest rising limb occurs with the non-moving scenario, which is true for all evaluation points. The order of the peak arrival for the other moving scenarios differs between the evaluation points. An upstream direction of movement generates the latest peak at evaluation point B, while the latest peak at point F and H occurs when the rainstorm has a downstream direction of movement. The difference between the earliest and the latest peak is 5 minutes at both evaluation point B and H, and the difference at point F is about 7 minutes.

The timing of the maximum water depth is totally consistent with the timing of the most intense rainfall. The lag time between the peak in the hyetograph to the maximum flood depth is almost constant in the scenarios, which can be seen in Figure 13 by comparing the dashed and dotted lines. The lag time is approximately 35 min at evaluation point B and F, and 59 min at point H. Hence, the lag time at evaluation point B, F and H is not affected by the storm movement.

4.1.2 Maximum flood depths

Figure 14 illustrates the distribution of the relative difference in maximum flood depths between a moving and a stationary rainstorm. The relative difference is defined as

$$\Delta H_m = \frac{H_m - H_{st}}{H_{st}} \cdot 100$$

where H_{st} is the maximum water depth for a given hyetograph and evaluation point with no movement and H_m is the flood depth under the same condition but where the rainstorm is moving. The equation above was applied for every hyetograph at all evaluation points which results in 60 values per histogram.

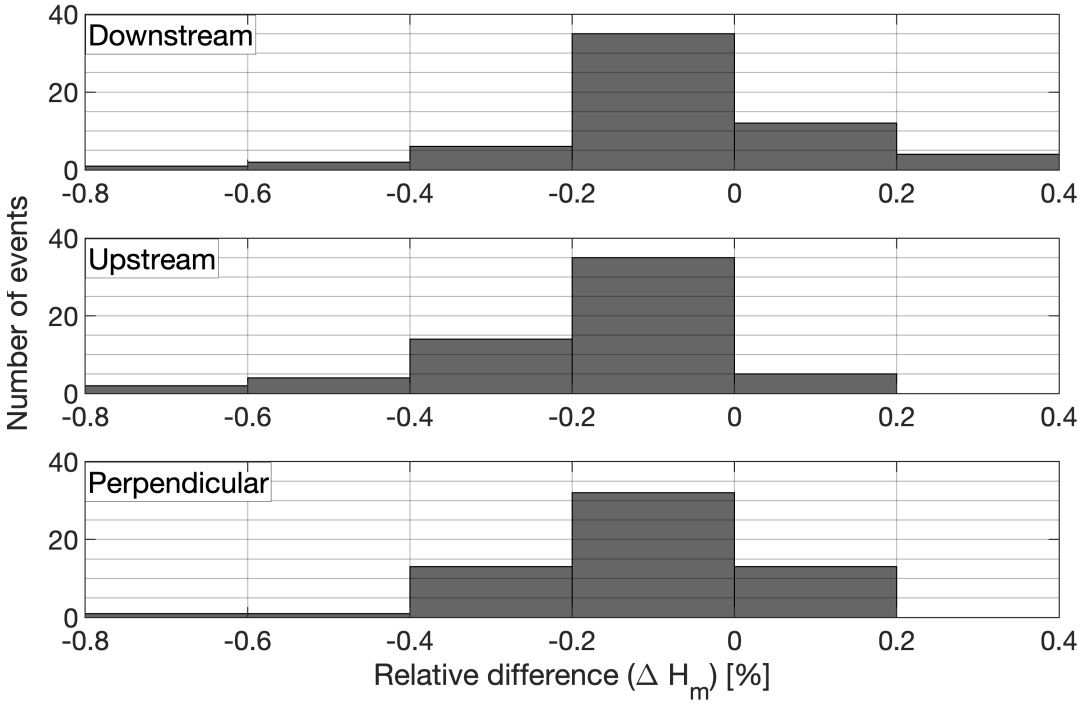

Figure 14. Distribution of the relative difference in maximum flood depth between a stationary and a moving rainstorm at all evaluation points for every hyetograph. Each plot illustrates how the maximum flood depth deviates when a rainstorm moves, compared to when it is stationary. A negative value indicates that the stationary scenario generates a higher water depth and vice verse.

The histograms in Figure 14 show that the flood depths generated in the moving scenarios vary less than 1% compared to when the rainstorm has no movement. A moving rainstorm tends to, in most of the cases, result in lower water levels. The variability is low though, more than 50% of the data set has a relative difference between 0% and -0.2 %. The downstream direction generates the most cases of water depths higher than a non-moving scenario, compared to the upstream and perpendicular direction. A downstream direction results in a relative difference up to 0.4% . The least likely direction to generate higher flood depths compared to a stationary rainstorm is the upstream direction, where only 5

instances had a water level greater than the non-moving scenario. Also, the water levels were only between 0% and 0.2% higher in those cases.

Figure 15 shows the distribution of the ratio between the maximum flood depth when the rainstorm moved downstream and when it moved upstream. The maximum flood depth is higher in two thirds of the events when the rainstorm moved downstream (H_D) compared to upstream (H_U). The amplification due to a downstream direction of movement varies in a wider range compared to the upstream direction. There is one event where the flood depth is 1% higher when the rainstorm moved downstream compared to when it moved upstream, but the ratio varies in general between 0.9985 and 1.003.

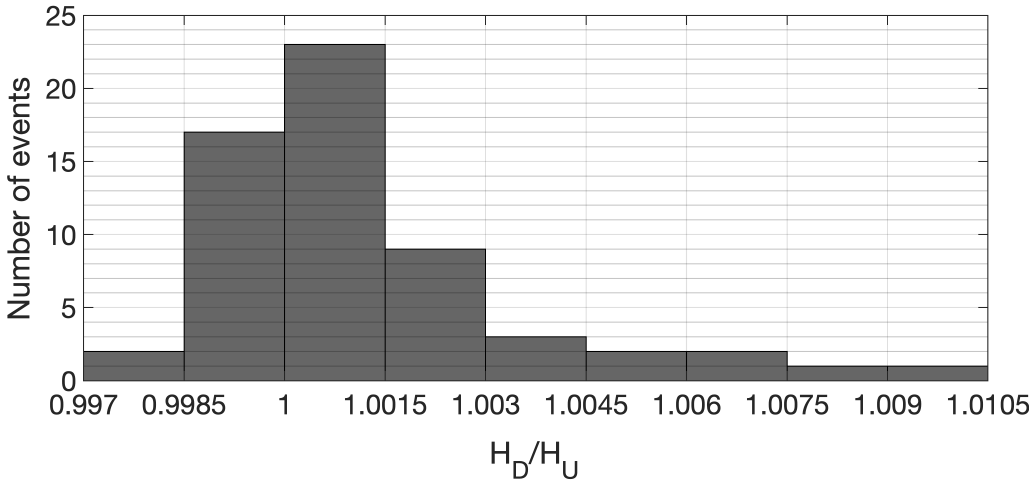

Figure 15. Distribution of the ratio in maximum flood depth between a downstream (H_D) and an upstream (H_U) direction of movement.

Figure 16 provides information on how the effect of storm movement varies between the evaluation points. The histograms in Figure 14 indicated that downstream is the most notable direction of movement with regard to amplified flood depths compared a stationary scenario, and Figure 16 shows that the biggest differences are concentrated to a few locations. Evaluation point E and I are two locations that exhibits an interesting behaviour. The maximum flood depths at these locations are higher when the rainstorm moves downstream compared to when it is stationary. Also, the hyetograph that resulted in the greatest relative difference when the storm moves downstream is in both cases Hyetograph number 5. When the rainstorm is moving in the opposite direction, the flood depths at point E and I are lower than the stationary scenario and a perpendicular direction results in the same depths as a stationary rainstorm. Evaluation points B, C, D and F show almost no sensitivity to storm movement with respect to maximum flood depth. The biggest relative difference in absolute terms is -0.7% and occurs at evaluation point F. Noteworthy is that all variation is in a small magnitude of order. As an example, if the flood depth in the stationary scenario is 50 cm and the relative difference is 0.2%, the absolute difference in flood depth is 1 mm.

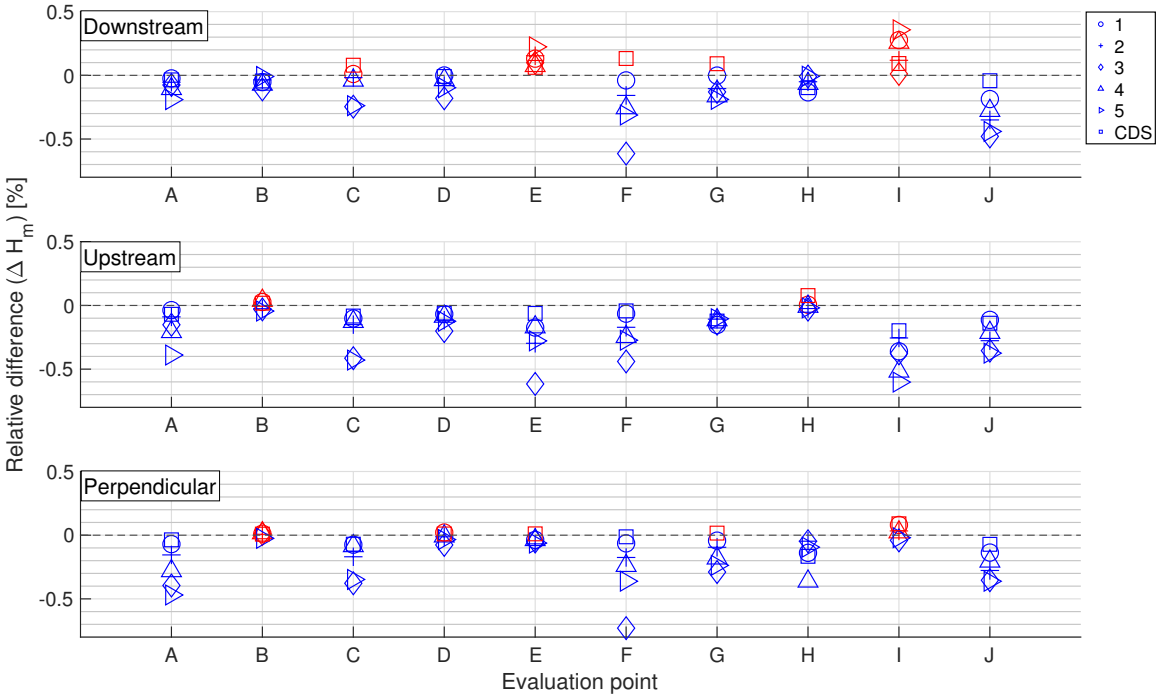

Figure 16. The relative difference in maximum flood depth at the evaluations points for all hyetographs, divided between the different directions of movement. The relative difference is defined as the difference between the flood depth for a stationary and moving scenario, normalized with the depth with the moving rainstorm. A negative value (blue) indicates that the flood depth is greater when the rainstorm is not moving, and a positive (red) means that the moving scenario generates a higher water depth.

4.2 THE EFFECT OF DIFFERENT HYETOGRAPHS

4.2.1 Maximum flood depth

One objective in this study was to investigate how the resulting flood depths vary with different hyetographs, i.e different temporal rainfall distributions. Figure 17 shows the maximum flood depth at the evaluation points with non-moving rainstorms. It was concluded in Section 4.1 that the influence of storm movement on maximum flood depth is of a very small order of magnitude which is the reason why only the results from the stationary scenarios are presented in this chapter. The reader is referred to Appendix F for data covering all scenarios.

It is clear from Figure 17 that the maximum flood depth, at the evaluated locations, is dependent on the hyetograph. The water level reaches at most approximately 0.5 m and the smallest depth, which occurs at evaluation point F, is around 0.15 m. The sensitivity to changes in the hyetograph differs between the evaluation points. The least difference in absolute terms is around 5 cm, which occurs at evaluation point B, while the greatest difference of around 20 cm occurs at E. The maximum flood depth at evaluation point E and F varies within a range where the highest water depth is almost double compared to

the lowest depth.

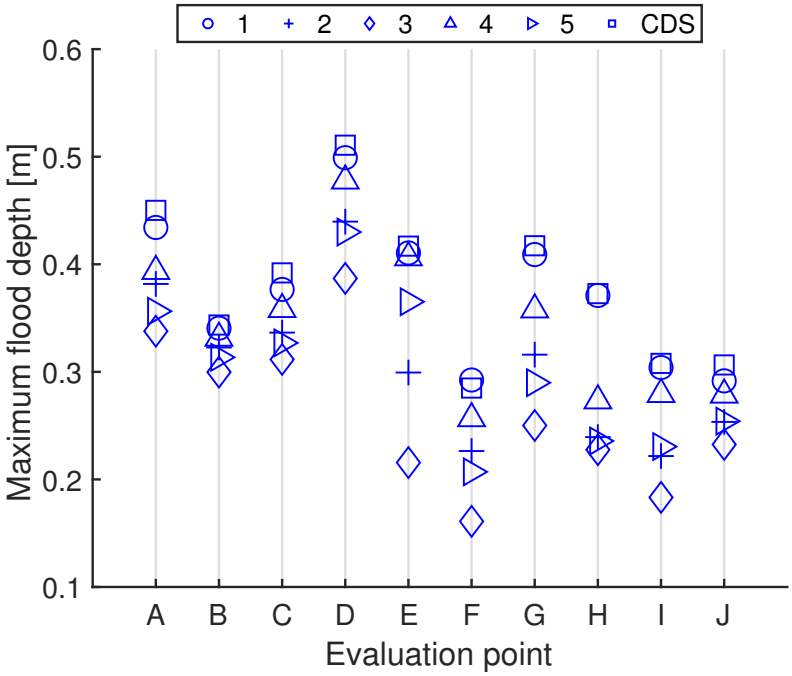

Figure 17. The maximum flood depth at the evaluation points generated by the different hyetographs with no storm movement.

Figure 18 visualizes how the maximum flood depth deviates from the mean depth, which is defined as

$$\Delta H_{mean} = \frac{H_{max} - H_{mean}}{H_{mean}} \cdot 100$$

where H_{max} is the maximum flood depth at a given evaluation point and hyetograph, and H_{mean} is the average flood depth at that evaluation point. The plot provides information of how sensitive the flood depth is to different rain patterns in relative terms. Furthermore, it clarifies which of the hyetographs that generates the highest flood depths at the evaluated locations. Evaluation point A, C, D and J shows a similar pattern, where the spread around the mean is approximately $\pm 15\%$. Figure 17 showed that the water depth at point B had the least variation in absolute terms, and Figure 18 shows that this is also true in relative measures. The results therefore indicate that evaluation point B is the least sensitive to different hyetographs. Evaluation point E, F, G, H and I seem to be most sensitive to different rain patterns, according to Figure 18. All of those locations, with the exception of H, are located on the eastern half of the model domain, see Figure 12. The widest spread around the mean depth occurs at evaluation point E and corresponds to a total of 57%. Noteworthy is that for the majority of the evaluation points, the negative and the positive spread around the mean is of the same size, implying that the depths varies rather consistently as a function of the different hyetographs.

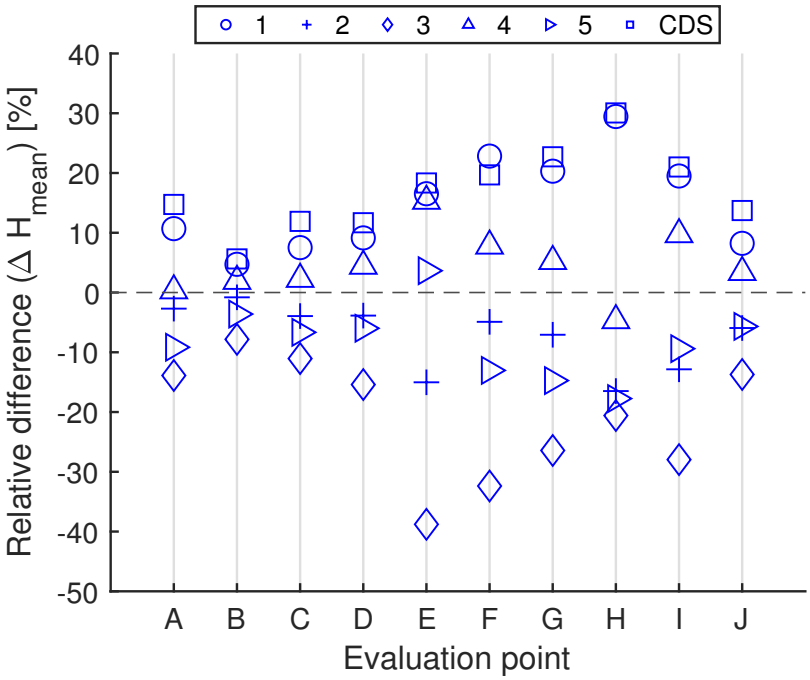

Figure 18. The relative difference in maximum flood depth at the evaluation points generated by the different hyetographs. The relative difference is defined as the difference between the flood depth and mean depth, normalized with the mean depth. A negative value indicates that the flood depth is lower than the mean value and vice verse.

In most of the cases, there are three hyetographs that generate a maximum flood depth greater than the mean and three that generate lower depths, which can be seen in Figure 18. The rank of which hyetograph that results in the greatest flood depth is also similar between the different evaluation points. The CDS-rain generates the highest values at nine of the ten evaluation points. The empirical hyetograph that generated the greatest flood depth is Hyetograph 1, where the result in many cases is around the same as for the CDS-rain. At evaluation point F though, Hyetograph 1 produced the greatest water depth compared to all of the other hyetographs. The hyetograph that generates the lowest flood depths is number 3, and it does so at every evaluation point. When comparing the flooding results from Hyetograph 2 and 5, there is no consistent pattern of which hyetograph that generates the highest water levels. Hyetograph 2 generates higher water depths than Hyetograph 5 at six locations, while the results from Hyetograph 5 is higher at two locations and the two hyetographs generates around the same flood depth at evaluation point H and J.

Table 3 summarizes the highest and lowest maximum flood depths and also the ratio between the them. The water depths are amplified with a factor between 1.15 and 1.93, with an average value of 1.51, when comparing the lowest and highest maximum flood depth.

Table 3. The highest and lowest maximum (peak) flood depth at the evaluation points, the ratio between the depths and which hyetographs that resulted in the values.

	Evaluation point									
	A	B	C	D	E	F	G	H	I	J
Max peak flood depth [cm]	45.0	43.4	39.2	51.1	41.7	29.2	41.7	30.8	30.8	30.6
Hyetograph	CDS	CDS	CDS	CDS	CDS	1	CDS	CDS	CDS	CDS
Min peak flood depth [cm]	33.8	30.0	31.2	38.7	21.6	16.1	25.0	22.8	18.3	23.3
Hyetograph	3	3	3	3	3	3	3	3	3	3
H_{max}/H_{min}	1.33	1.15	1.26	1.32	1.93	1.82	1.67	1.64	1.68	1.32

4.2.2 Flood depth variation over time

The flood response, in terms of water level, for different hyetographs at evaluation point D is plotted in Figure 19. That location was exposed with the greatest flood depth (Figure 17) and is therefore highlighted in this section. See Appendix G for plots of all evaluation points.

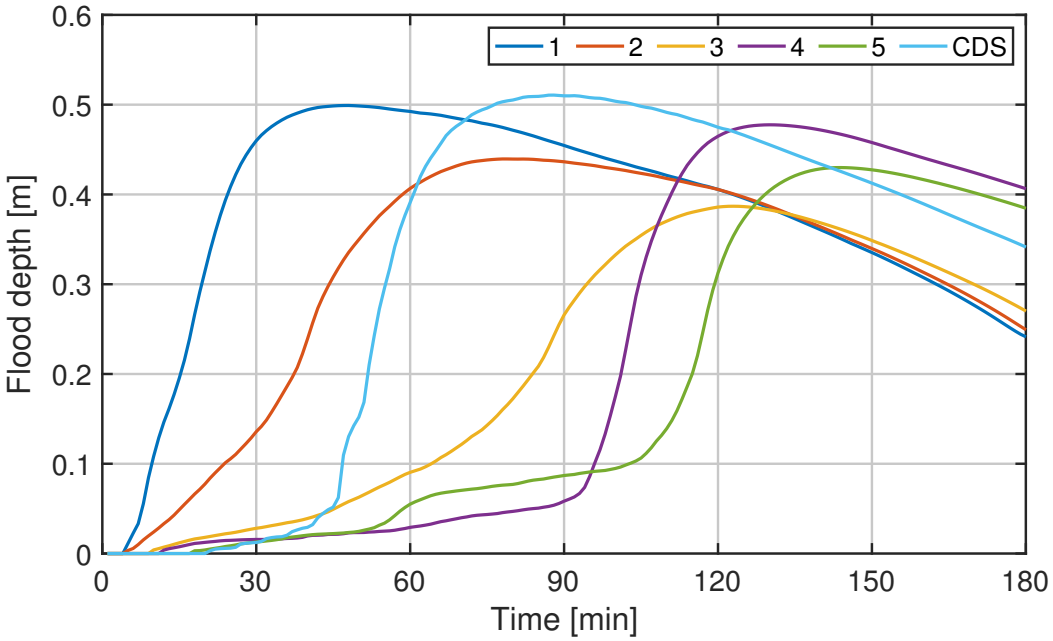

Figure 19. Flood depth as a function of time at evaluation point D for all hyetographs with a non-moving rainstorm.

The curve for Hyetograph 1 shows an immediate, rapid and almost constant rise in flood depth, followed by a slower recession after the maximum depth is reached. The flood depth with both the CDS-rain and Hyetograph 4 increases at a similar rate as with Hyetograph 1, although the slope is not as steep in the initial response. The latter is especially true for Hyetograph 4, where the flood depth increases slowly for about 90 minutes until a much faster progression starts. This dynamic is also the case for Hyetograph 5, which has two phases where the flood depth increases slowly. Hyetograph 3 generates the overall

slowest response in flood depth.

There is a big difference in the arrival of the maximum flood depth between the different hyetographs. The earliest peak is generated by Hyetograph 1 and the latest occurs when Hyetograph 5 is simulated. The difference in time is about 100 minutes between the earliest and the latest peak.

4.3 COMPARISON OF FLOOD DEPTHS FROM EMPIRICAL HYETOGRAPHS AND CDS-RAIN

A CDS-rain was used as rain input in order to evaluate how the flood depths differ from those generated by the empirical rain hyetographs. In Figure 20 is the relative difference in maximum flood depth between the CDS-rain and the empirical hyetographs for stationary rainstorms plotted. The figure resembles the characteristics from Figure 17, but is focused on the difference between the CDS-rain and the other hyetographs. The relative difference is defined as

$$\Delta H_{CDS} = \frac{H_{EH} - H_{CDS}}{H_{CDS}} \cdot 100$$

where H_{CDS} is the maximum flood depth with the CDS-rain and H_{EH} is the maximum depth generated by an empirical hyetograph.

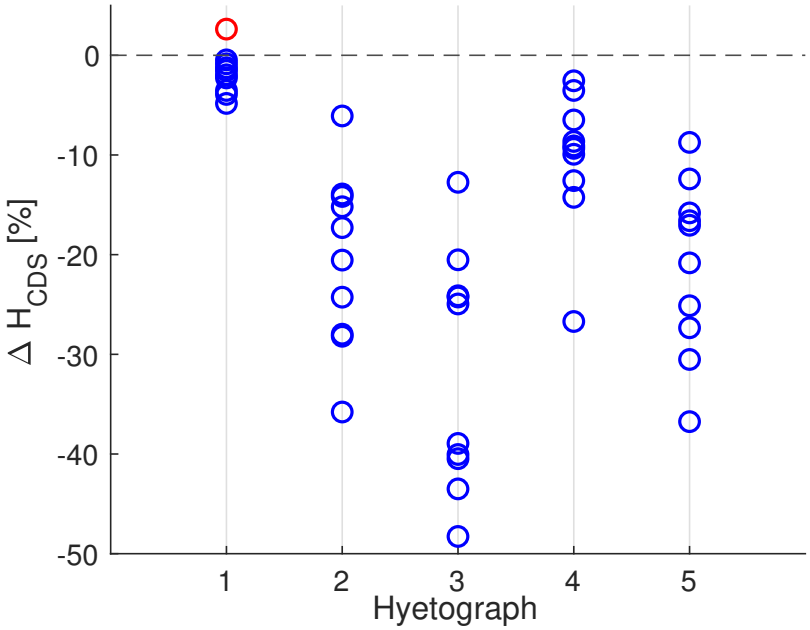

Figure 20. The relative difference in maximum water depth at the evaluation points between the CDS-rain and the empirical rain shapes, for stationary rainstorms. The relative difference is defined as the difference in flood depth between the CDS-rain and an empirical rain shape, normalized with the flood depth for the CDS-rain. A negative value (blue) indicates that the CDS-rain generates greater flood depths, and a positive (red) means that the empirical rain shape generates higher water depth.

Hyetograph 1 produced water depths, at the evaluated locations, similar to the CDS-rain, as seen in Figure 20. The water depth with Hyetograph 1 is at one point (evaluation point E) greater than the CDS-rain, with a difference of around 3%. For the rest of the occasions, the relative difference ranges between 0 and -5% for Hyetograph 1. The resulting water levels when hyetograph 2–5 are simulated are considerably lower compared to the CDS-rain. Hyetograph 2 and 5 generate water depths that differs in a similar way. The relative difference for those hyetographs ranges between around -6 and -37%. The water level generated by Hyetograph 3 is at one instance almost half of the water level from the CDS-rain. Hyetograph 4 generates the second least relative difference and ranges between -3 and -38%.

5 DISCUSSION

The aim of the study has been to investigate flooding phenomena forced by extreme rainfall in an urban environment. The objective has not been to evaluate the flooding consequences in the study area specifically, the site has been utilized as a tool to achieve the aim of the study. Emphasis should be put on that the characteristics of the catchment and stormwater infrastructure influence the results. Extrapolating the results of this study to other situations should therefore be done with caution. The remaining of this chapter will interpret, discuss, and relate the results to previous research, address the computational performance of the model and uncertainties in the model set-up.

5.1 THE INFLUENCE OF STORM MOVEMENT ON MAXIMUM FLOOD DEPTH

The effect of storm movement on maximum flood depths in the study area was of a magnitude that most likely do not have any practical implications. The relative difference between a moving and a stationary scenario were greatest for the eastern movement and was between -0.8% and 0.4%, which can be seen in Figure 10. East is the most downstream direction and could be expected to produce greater difference in flood depths compared to a stationary rainstorm since previous research has shown how the movement affects the catchments response (e.g. Niemczynowicz 1984, Yen & Chow 1969, de Lima & Singh 2002). The more upstream direction, west, generated the least amount of instances where the moving scenario produced greater water depths compared to a stationary scenario. This further indicates that a downstream direction of storm movement can amplify the maximum flood depths, although in a small extent, compared to an upstream direction.

An interesting result is that the stationary rainstorms generated the greatest flood depths at almost all evaluation points compared to the moving scenarios. It is hard though to find an explanation for this result based on the evaluated parameters in this study. One cause might be that the total time of rainfall differs between the stationary and the moving scenarios. For a stationary rainstorm, it will rain for 2 hours over the whole model domain, but in the moving scenarios it will rain somewhere in the model domain for 8 minutes longer due to time lags. This implies a longer rain duration if the whole catchment is considered, although it will rain for 2 hours on a grid cell level. Other explanations could be that a homogeneous rainfall over the area does produce greater flood response or that the difference between storm speed (8 m/s) and flow speed (mostly lower than 1 m/s) was too large.

The characteristics of the moving rainstorms in this study may have affected the possible impact on the maximum flood depths. Previous research points out factors for runoff amplification due to storm movement. One important factor is the storm speed, which should be similar to the flow speed in order to have the largest impact on the peak discharge (Yen & Chow 1969; Ngirane-Katashaya & Wheater 1985; Seo et al. 2012; Volpi et al. 2013). The storm speed in this study was set to 8 m/s which is much higher than the average surface flow speed in the simulations. Figure C.1 shows that the model domain is dominated by maximum flow speeds lower than 0.2 m/s, which can be explained by the rural areas surrounding the urbanized center. The highest flow speeds were between 0.5–1.7 m/s and were concentrated to spots in the bathymetry where buildings are represented, while speeds between 0.2 and 0.5 m/s are more associated with roads and similar structures. The magnitude of the flow speeds are in line with literature values which, according to for example Svenskt Vatten (2011) is 0.1 and 0.5 m/s for natural vegetation and gutters, respectively. The maximum flow speed only occurs instantaneously, hence averaged values were also analyzed. The weighted mean of the maximum flow speed in a delimited urban area was 0.29 m/s and 0.10 m/s when averaged over the maximum flow speed and the average speed of the first hour, respectively. The average flow speed in the whole domain were considerably lower, due to the vast area of non hardened surfaces in the model domain. The average maximum flow speed upstream evaluation point I were 0.45 m/s, which is an interesting measure since a coherent segment of surface flow is more likely to develop a resonance effect. The implemented storm speed was considered a good representation of the average speed for a convective rain cell. Also, since other rain related parameters were altered between the simulation runs, it would not have been possible to also investigate the influence of different storm speeds within the time frame of this study.

It should be noted that the articles mentioned in the paragraph above have approached the influence of storm movement by using mathematical approaches, conceptualized catchments and laboratory experiments. It is likely that the complexity of the catchment in this study would reduce the effect of storm movement. Veldhuis et al. (2018) used observed peak flows from 279 events from five urban catchments to partially study the role of storm movement in urban flooding. The size of the basins ranged between 7–111 km^2, which means that the smallest catchment is of similar size as the site in this study. The authors did not find any significant impact on the peak flows depending on the storm's movement. Actually, slow moving and stationary rainstorms tended to produce greater flood peaks compared to faster moving rainstorms, which is in line with the results in this study. A similiar conclusion was drawn by Nikolopoulos et al. (2014) when two hydrological models of a large non-urban catchment were studied. Although those studies relate to pluvial processes and no general conclusion can be drawn from them, they further emphasize on the complexity of extrapolating theoretical relationships to the dynamics of real situations. Furthermore, it strengthens the argument that the influence of storm movement in this study was limited by the high storm speed.

5.2 THE INFLUENCE OF DIFFERENT HYETOGRAPHS ON MAXIMUM FLOOD DEPTH

All evaluated locations showed a sensitivity to changes in the hyetograph with respect to maximum flood depth. While the influence of storm movement was found to be negligible, a change in the hyetograph had a considerable influence on maximum flood depths. At one evaluated location, the maximum flood depth increased 1.9 times when comparing the results from two different hyetographs while keeping the total rainfall depth constant.

As seen in Figure 17, the flood depths varied depending the hyetograph, but also between the different evaluation points. Evaluation point D, located in the north eastern quadrant of the model domain, experienced the greatest flood depth which was at most 51.1 cm (Table 3). The lowest flood depth occurred at evaluation point F, which is located far out in the eastern part of the model domain and characterized by a rural landscape. This is probably a result of the lack of hardened surfaces and therefore a slower runoff process and better opportunity for infiltration. The objective though was not to find the most critical locations with regard to the absolute flood depth, but to see how the maximum flood depth varies with different temporal distributions of rainfall intensities. The ratio between the highest and the lowest maximum flood depth at the evaluation points ranged between 1.15 and 1.93, with an average value of 1.51 (Table 3). The biggest increase in maximum flood depth occurred at evaluation point E, where the maximum flood depth increased from 21.6 to 41.7 cm. It is hard to find an explanation for why point E experience the biggest variation due to the complex runoff process with the surface heterogeneity and stormwater infrastructure. The location of evaluation point D has similar characteristics as point E, but is not as sensitive to different hyetographs. Both evaluation points are located downstream in the model domain and are close to a manhole which is connected to a branching stormwater pipe. There is a tendency, with the exception of evaluation point G, for larger variation in maximum flood depth in the eastern half of the model domain compared to the western part (Figure 18). In order to draw any general conclusion from this, a more extensive analysis of the spatially distribution of the variations in flood depths need to be performed.

The hyetograph that generated the greatest maximum flood depth at all but one evaluated locations was the CDS-rain (e.g. Figure 17). This result suggest that there is a risk of overestimating flood depths with the current modelling practice, since the empirical hyetographs are a better representation of real rain events in Sweden compared to a CDS-rain. Although it should be noted that a late arrival of the peak intensity is not as likely as an early peak when considering heavy rainfalls (Olsson et al., 2017). This implies that the risk of overestimating flood depths when using the CDS-rain as model input might be reduced, since Hyetograph 3, which resulted in the lowest flood depths, is not as likely to occur as Hyetograph 1, which produced the greatest flood depths.

Hyetograph 1 generated the second greatest flood depths and was therefore the empirical hyetograph that resulted in highest flood depth. This is an unexpected result considering that the hyetograph has an early peak compared to the other empirical rain shapes, and a later peak have been found to be associated with higher flood peaks due to less surface retention (Mazurkiewicz & Skotnicki 2018a; Šraj et al. 2010). Figure D.1 in Appendix D

illustrates the moisture content in the model domain before the peak intensity in Hyetograph 1 and 4 arrives. It is clear that the rain volume that precedes the peak in Hyetograph 4 (Figure 4) increases the water content in the soil more than in the case with Hyetograph 1, but not to an extent where the soil layer becomes saturated. If that would be the case, it is possible that the hyetographs with a later peak would have resulted in higher flood depths. An improvement of the study would be to conduct a sensitivity analysis with respect to the initial soil moisture. This was not possible to proceed with due to the limited time frame. Furthermore, Šraj et al. (2010) points out that the location of the intensity peak has a greater influence on the timing of the maximum discharge than on the absolute value. The results in this study confirms that this conclusion also applies for maximum flood depth. This can be seen in Figure 19 where the maximum depth arrival follows the order of whichever hyetograph that has an earlier peak.

The results in this study suggest that a large amount of rainfall within a short period of time is a more important factor than the location of the peak intensity when evaluating maximum flood depths. This can be derived from the fact that Hyetograph 1 produced greater flood depths than Hyetograph 4 and 5 which have much later peaks. When analyzing the rainfall depth during the peak of Hyetograph 1 in Figure 4, around 70% of the total depth is released during the peak which corresponds to about 25 minutes. Hyetograph 4 on the other hand, only has 60% of the total depth orientated around the last 30 minutes and Hyetograph 5 has even less. The smaller amount of rain within the peak is probably the reason why Hyetograph 4 and 5 generate lower flood depths than Hyetograph 1 even though they have a later peak. The CDS-rain, which generates the highest flood depths in general, has a slight lower rain amount during it's most intense 25 minutes compared to Hyetograph 1, indicating that the relationship between short intense rainfall and flood depth is not straightforward. A possible explanation to why the CDS-rain generated greater flood depths might be associated with the later peak compared to Hyetograph 1. The results discussed above indicate that the magnitude and the location of the peak is not the only important hyetograph characteristics when evaluating flood response, the overall shape also needs to be considered.

Hyetograph 3 generated the lowest flood depths in all scenarios. The hyetograph is characterized by not having a distinct peak, instead it has an elongated peak that stretches over half of the duration with a maximum intensity in the last third of the duration. The distribution of rainfall in Hyetograph 3 have similarities with a blockrain, which has a constant rainfall throughout the duration. The results in this study therefore indicate that flood depths can be overestimated when using a blockrain instead of a hyetograph with temporal variability.

5.3 COMPUTATIONAL PERFORMANCE AND VALIDITY

Both MIKE URBAN and MIKE 21 provide tools for monitoring the computational performance of the simulation. One approach is to check if the Courant Number is below 1, which is a good measure of stability for the MIKE 21 model (DHI, n.d). The Courant Number was well below 1 in all simulations and the model can therefore be considered as stable with the input parameters used in this study.

The MIKE software takes measures to maintain model stability which can result in mass balance violations (DHI 2017b; DHI 2017d). Water is artificially generated if the water level falls below a certain threshold. Table H.1 summarizes the water level corrections and shows that it is present in all scenarios. The water level correction in the MIKE 21 model ranged between 21021 and 46289 m^3 which corresponds to 5–11 % of the total precipitation volume. The error correction varies more between the different hyetographs than between the different storm directions for a single hyetograph. This means that the comparison of maximum flood depths between different directions might be more valid than the comparison between different hyetographs, if error correction would have an significant effect on the modelling outcome. The error correction is closely related to the infiltration module in MIKE 21. If the infiltration capacity is high enough to infiltrate all available water in a grid cell, it will be fully drained and MIKE 21 will reset the water level to a default value of 0.2 mm (DHI, 2017b). It is therefore likely that this process occurs at time steps where the precipitation is low and in areas that receive little water from neighbouring cells. The water level correction in the MIKE 21 model is not considered an issue since it is not likely to affect the inundated locations that has been evaluated in this study. Furthermore, no relationship between scenarios with high water correction and high flood depths seems to be present.

The MIKE URBAN model also added artificial water in all simulations. The amounts are significantly lower than in the MIKE 21 model due to the smaller scale of the system. The minimum water depth in MIKE URBAN is by default 20‰ of the link diameter, but has a maximum value of 20 mm (DHI, 2017d). If the water level in a link drops below this threshold, MIKE URBAN will add water. This implies that dry parts of the system will experience this violation of the mass balance. Table H.1 in Appendix H confirms this, since a later peak in the hyetograph results in an increased amount of water correction. It is clear from Table H.1 that the water correction is a function of the location of the peak, a later peak generates more artificial water. As an example, Hyetograph 5 has a much later peak than Hyetograph 1, meaning that the flow in the collection system will be delayed in comparison. Hence, there will be more time for water level correction which results in greater correction volumes. Since this only occurs during time steps with very low flows, it is not considered to bias the results. The minimum water depth can be changed by the user and one aspect to be investigated in a future study could be a sensitivity analysis where the minimum water depth is altered. Another approach would be to use a base flow in all simulations to see if the water correction has any influence on the maximum flood depths.

A challenge in flood modelling is to validate the results. This is especially true for events with long return periods due to the lack of validation data (Neal et al., 2012). Also, calibration of the model is important in order to find parameter values so that the model can make accurate predictions. These measures have not been applied in this study due to mainly two reasons. Firstly, no data from an event of the same magnitude as in this study has been available. Secondly, the scope of this study has been to investigate relative difference which makes the occurrence of a potential bias less important since it is present in all scenarios. To further strengthen the findings, the methodology developed in this study could be applied to a 1D-2D model that has been calibrated and validated against

observed data.

One risk with evaluating the flood response at certain locations is that important results might be overlooked. In order to evaluate how well the results from the evaluation points reflects the behaviour at all locations in the study area, a map of difference in maximum flood depth between the CDS-rain and Hyetograph 3 was created, see Figure B.1. The majority of the evaluation points are located at spots which have the largest differences in flood depth, when considering the urban areas. There are locations with larger differences present, but many of these flooded areas could not meet the criteria for being an evaluation point. The evaluation approach in this study is therefore considered an adequate methodology.

5.4 THE MODEL SET-UP

The implementation of the moving and stationary rainstorms results in an implication that should be emphasized. The storm movement was implemented by mapping the same hyetograph with different time lags to each of the grid cells. This implies that the rain cell has a constant temporal distribution of rainfall intensity. If the same rain cell instead would be stationery, all grid cells would experience a constant rainfall. The stationary rainstorm was modelled with a temporal variability, meaning that the rainfall intensity in the cloud varies with time. Note that that all grid cells were exposed with the same amount of rain and the same distribution of rainfall intensity. The scenarios are therefore considered to be comparable, although there is a discrepancy in the rainstorm properties if the modelled rain cell is viewed as a real system.

The dynamics of the water flow in the 1D model of the stormwater drainage system is dependent on how the rain is divided between the coupled models. Impervious surfaces such as rooftops are usually directly connected to the drainage network and most often represented in the 1D model (MSB, 2017). A rain that equals the capacity of the collection system is then loaded onto these surfaces while the 2D terrain model is loaded with the remaining rainfall depth. If this is not modeled, the water will flow off the roof and be diverted by the slope of the topography, which not necessarily means the direction of the nearest manhole. In this study, the terrain model was loaded with all the precipitation which might lead to both underestimated and delayed flows in the collection system. The decision to not divide the precipitation between the models was purely due to practical reasons. No reasonable method for an implementation of the storm movement while dividing the precipitation between the two models could be found and elaborated in this study. The effect of the possible delayed and underestimated pipe flows on the results is not considered to be significant since the bias from the rain implementation is present in all scenarios. Also, the flow peaks in the drainage network were captured within the time of simulation.

The MIKE URBAN model could be modified to better represent the stream network that flows in the northern part of the study area. Sections of the streams that do not flow through a culvert is represented in the MIKE URBAN model as open channels. The streams are also captured by the DEM (Figure 9) and therefore represented in the MIKE 21 model. A consequence of this is a double flow, one flow in the MIKE URBAN model

and one in the MIKE 21 model. There are few coupling nodes along the streams which makes the water exchange between the models limited. This could be a critical aspect when considering possible resonance effects since large volumes of water flows through these conduits. No evaluation point are located near the streams and should therefore not be directly influenced by this. A future model improvement could be to increase the number of coupled nodes along the streams or to use nodes that allow for lateral water exchange.

The bed resistance in the terrain model was only differentiated by two values, 50 $m^{1/3}$/s and 2 $m^{1/3}$/s. This approach is a simplification since the real surface conditions consist of a wide spectrum of different surface types. A more realistic model might have been the result if the Manning's values were even further differentiated. The values that were used are, according to Gustafsson & Mårtensson (2014), considered a good representation of the bed resistance when only single values to hardened and non hardened surfaces. The values are empirically derived and different values can be found in the literature. As an example, Chow et al. (1988) specifies 20 $m^{1/3}$/s for light bush and weeds and 77 $m^{1/3}$/s for smooth asphalt, while Vägverket (2008) states 30–35 $m^{1/3}$/s and 88–85 $m^{1/3}$/s for short grass and smooth asphalt, respectively. The value that was used for the hardened surfaces might therefore seem too low. Gustafsson & Mårtensson (2014) showed that the Manning value is a critical parameter in hydraulic modelling, but even though the bed resistance is an important aspect in hydraulic modelling, the modeled bed resistance is not considered to influence the results of this study considerably. This due to the consistent bed resistance in all scenarios and that there is a good distinction between hardened and non hardened surfaces.

5.5 THE EMPIRICAL HYETOGRAPHS

Olsson et al. (2017) points out that previous studies on rain event's temporal distribution have been quite few internationally and especially in Sweden. Only one Swedish publication is mentioned. It has therefore been well motivated to study the updated survey conducted by Olsson et al. (2017). The empirical hyetographs provide new information about the location of the peak, the overall shape and how frequent the different shapes are. As shown in this study, the overall shape of the hyetograph has a great influence on the flood response. From a design practice point of view, this study provides insight on how the flooding from the empirical hyetographs relate to the design storm of today - the CDS-rain.

There are some aspects of the data set behind the empirical rain shapes that are relevant to point out. The data set behind Olsson et al. (2017) analysis consists of rain events that has an average intensity of at least 6 mm/h, which is considerably lower than the 32.6 mm/h that has been used in this study. The empirical hyetographs does therefore not only reflect extreme rains, but also rain events that SMHI classifies as moderate showers (SMHI, 2015). To address this, Olsson et al. (2017) analyzed the most extreme rainfalls in the data set with respect to the different empirical rain shapes. It turns out that, for long rainfalls, the peak tends to be located in the first half of the duration (Hyetograph 1 and 2). In fact, the occurrence of the first two hyetographs were almost three times higher compared to hyetograph 4 and 5. This is an interesting finding since Hyetograph

1 generated the highest flood depths among the empirical hyetographs. The findings by Olsson et al. (2017) strengthens the design practice of today, which is to place the peak at 32–48% of the duration (Svenskt Vatten, 2011).

There are factors of uncertainty related to the empirical rain shapes. The variability around the mean intensity at each time step is relatively high, especially around the peak, which can be seen in Figure 3. The exact location of the maximum intensity is therefore uncertain. Considering the variability, the peak could arrive somewhere in the interval where the majority of the rainfall is produced. Noteworthy is also that 133 rainfall events make up the data set that generated the five different hyetographs, which means that the data availability is limited. To further analyze the temporal distribution of rainfall in a Swedish context, it would be an improvement if the findings in Olsson et al. 2017 were complemented with data from more gauges or radar measurements.

6 CONCLUSIONS

The influence of storm movement and temporal distribution of rainfall on urban pluvial flooding was investigated by forcing a 1D-2D model of an urban study area with different rain scenarios. Five empirical hyetographs developed by Olsson et al. (2017) and one CDS-rain were used as rain input. Maximum flood depths were evaluated at ten locations and the following conclusions can be drawn.

- Storm movement had negligible effect on maximum flood depth at all evaluated locations. The relative difference in maximum flood depth between a moving and a stationary rainstorm varied in the vast majority of the cases with less than 0.5%. The temporal distribution of rainfall intensity had considerable effect on the flood depths. The maximum flood depth was at most amplified by a factor of 1.9 when comparing flood depths produced by two different hyetographs. Thus, storm movement is not as critical as hyetograph characteristics with respect to maximum flood depths in urban pluvial flooding.

- The CDS-rain generated the highest maximum water depths at all but one evaluation point. One empirical hyetograph had similar outcome as the CDS-rain, while the other four resulted in considerably lower flood depths. There is therefore a risk of overestimating flood depths when using a CDS-rain like the one in this study as model input.

Although storm movement did not have an important influence on the maximum flood depths, it was found that a stationary rainstorm resulted in slightly higher flood depths (0.7% at most) compared to the moving scenarios. Furthermore, some indication on that a downstream direction had the greatest effect compared to other directions was found. It was not possible to validate the model results due to the lack of observations. A continuation of this study could be to apply the methodology to a validated hydraulic model. The results in this study suggest that it is not necessary to include storm movement in hydraulic design practice. However, the selection of hyetograph has great influence on the modelling result.

REFERENCES

Akan, O. A. och Houghtalen, J. R. (2003) *Urban hydrology, hydraulics, and stormwater quality: Engineering applications and computer modeling*. New Jersey, United States: John Wiley & Sons.

Alfieri, L., Laio, F. och Claps, P. (2008). A simulation experiment for optimal design hyetograph selection. *Hydrological Processes*, , vol. 22, p. 813–820, DOI: http://dx.doi.org/10.1002/hyp.6646.

Bai, Y., Zhang, Z. och Zhao, W. (2019). Assessing the impact of climate change on flood events using HEC-HMS and CMIP5. *Water, Air, & Soil Pollution*, , vol. 230, p. 119, DOI: http://dx.doi.org/10.1007/s11270-019-4159-0.

Bezak, N., Šraj, M., Rusjan, S. och Mikoš, M. (2018). Impact of the rainfall duration and temporal rainfall distribution defined using the huff curves on the hydraulic flood modelling results. *Geosciences*, , vol. 8, p. 69, DOI: http://dx.doi.org/10.3390/geosciences8020069.

Chow, V. T., Maidment, D. R. och Mays, L. W. (1988) *Applied Hydrology*. Singapore: McGraw Hill.

de Lima, J. och Singh, V. (2002). The influence of the pattern of moving rainstorms on overland flow. *Advances in Water Resources*, , vol. 25, p. 817–828, DOI: http://dx.doi.org/10.1016/S0309-1708(02)00067-2.

DHI (2016) MIKE Powered by DHI FAQ. Available from: https://faq.dhigroup.com/default.asp?module=MIKE+URBAN&ID=456#answer [2019-03-26].

DHI (2017a) MIKE FLOOD User Manual.

DHI (2017b) MIKE Flow Model User Guide.

DHI (2017c) MIKE URBAN Collection System User Guide.

DHI (2017d) MOUSE Pipe Flow Reference Manual.

DHI (n.d.) MIKE 21 - 2D modelling of coast and see. Available from: http://www.mikepoweredbydhi.com/products/mike-21 [2019-01-21].

DHI (n.d) MIKKE 21 Flow Model - Hints and recommendations in applications with significant flooding and drying.

ESRI (2011) ArcHydro Tools 2.0: Tutoral. Available from: http://downloads.esri.com/archydro/archydro/ [2019-04-01].

Gustafsson, L. G. och Mårtensson, E. (2014). Kartläggning av skyfalls påverkan på samhällsviktig verksamhet: Framtagande av metodik för utredning på kommunal nivå. *MSB694*, , p. 64.

Hernebring, C. och Mårtensson, E. (2013). Pluviala översvämningar: Konsekvenser vid skyfall över tätorter. *MSB567-13*.

Hernebring, C., Milotti, S., Kronborg, S. S., Wolf, T. och Mårtensson, E. (2015). Skyfallet i sydvästra skåne 2014-08-31: FokuSerat mot konsekvenser och relation till regnstatistik i Malmö. *Vatten - Journal of Water Management and Research*, , vol. 2015-2, p. 85–100.

Hettiarachchi, S., Wasko, C. och Sharma, A. (2018). The role of storm temporal patterns. *Hydrology and Earth System Sciences*, , vol. 22, p. 2041–2056, DOI: http://dx.doi.org/10.5194/hess-22-2041-2018.

Jha, A. K., Bloch, R. och Lamond, J. (2012) *Cities and Flooding: A guide to integrated urban flood risk management for the 21st century*. Washington DC, United States: World Bank Publications.

Keifer, C. J. och Chu, H. H. (1957). Synthetic storm pattern for drainage design. *Journal of the Hydraulics Division*, , vol. 83, p. 1–25.

Koutsoyiannis, D., Kozonis, D. och Manetas, A. (1998). A mathematical framework for studying rainfall intensity-duration-frequency relationships. *Journal of Hydrology*, , vol. 206, p. 118–135, DOI: http://dx.doi.org/10.1016/S0022-1694(98)00097-3.

MacKay, D. J. C. (2002) *Information theory, inference & learning algorithms*. New York, United States: Cambridge University Press.

Mark, O., Weesakul, S., Apirumanekul, C., Aroonnet, S. B. och Djordjević, S. (2004). Potential and limitations of 1D modelling of urban flooding. *Journal of Hydrology*, , vol. 299, p. 284–299, DOI: http://dx.doi.org/10.1016/j.jhydrol.2004.08.014.

Mazurkiewicz, K. och Skotnicki, M. (2018a). A determination of the synthetic hyetograph parameters for flow capacity assessment concerning stormwater systems. *E3S Web of Conferences*, , vol. 45, DOI: http://dx.doi.org/10.1051/e3sconf/20184500053.

Mazurkiewicz, K. och Skotnicki, M. (2018b). The influence of synthetic hyetograph parameters on simulation results of runoff from urban catchment. *E3S Web of Conferences*, , vol. 30, DOI: http://dx.doi.org/10.1051/e3sconf/20183001018.

Moseley, C., Berg, P. och Haerter, J. O. (2013). Probing the precipitation life cycle by iterative rain cell tracking: Convective rain in lagrangian view. *Journal of Geophysical Research: Atmospheres*, , vol. 118, p. 13,361–13,370, DOI: http://dx.doi.org/10.1002/2013JD020868.

MSB (2017). Vägledning för skyfallskartering: Tips för genomförande och exempel på användning. *MSB1121*.

Neal, J., Schumann, G. och Bates, P. (2012). A subgrid channel model for simulating river hydraulics and floodplain inundation over large and data sparse areas. *Water Resources Research*, , vol. 48, DOI: http://dx.doi.org/10.1029/2012WR012514.

Ngirane-Katashaya, G. G. och Wheater, H. S. (1985). Hydrograph sensitivity to storm kinematics. *Water Resources Research*, , vol. 21, p. 337–345, DOI: http://dx.doi.org/10.1029/WR021i003p00337.

Niemczynowicz, J. (1984). Investigation of the influence of rainfall movement on runoff hydrograph: Part I – simulation on conceptual catchment. *Nordic Hydrology*, , vol. 15, p. 71–84.

Nikolopoulos, E. I., Borga, M., Zoccatelli, D. och Anagnostou, E. N. (2014). Catchment-scale storm velocity: Quantification, scale dependence and effect on flood response. *Hydrological Sciences Journal*, , vol. 59, p. 1363–1376, DOI: http://dx.doi.org/10.1080/02626667.2014.923889.

Olsson, J., Berg, P., Eronn, A., Simonsson, L., Södling, J., Wern, L. och Yang, W. (2017). Extremregn i nuvarande och framtida klimat. *Klimatologi*, , vol. 47.

Olsson, J. och Josefsson, W. (2015). Skyfallsuppdraget: ett regeringsuppdrag till SMHI. *Klimatologi*, , vol. 37.

Prodanovic, P. och Simonovic, S. P. (2004) Generation of synthetic design storms for the Upper Thames River Basin CFCAS Project: Assessment of water resources risk and vulnerability to changing climate condition. Project Report V, The University of Western Ontario, Ontario, Canada. Available from: https://www.eng.uwo.ca/research/iclr/fids/publications/cfcas-climate/reports/Report%20V.pdf [2019-02-15].

SCB (2018a) Befolkning i tätorter 2017. Available from: https://www.scb.se/hitta-statistik/statistik-efter-amne/miljo/markanvandning/tatorter/pong/statistiknyhet/befolkning-i-tatorter-2017/ [2019-02-15].

SCB (2018b) Tätorter. Available from: https://www.scb.se/MI0810 [2019-04-01].

Seo, Y., Schmidt, A. R. och Sivapalan, M. (2012). Effect of storm movement on flood peaks: Analysis framework based on characteristic timescales. *Water Resources Research*, , vol. 48, DOI: http://dx.doi.org/10.1029/2011WR011761.

da Silveira, A. L. L. (2016). Cumulative equations for continuous time Chicago Hyetograph Method. *RBRH*, , vol. 21, p. 646–651, DOI: http://dx.doi.org/10.1590/2318-0331.011615094.

Singh, V. P. (1997). Effect of spatial and temporal variability in rainfall and watershed characteristics on stream flow hydrograph. *Hydrological Processes*, , vol. 11, p. 1649–1669.

Sivapalan, M. och Blöschl, G. (1998). Transformation of point rainfall to areal rainfall: Intensity-Duration-Frequency curves. *Journal of Hydrology*, , vol. 204, p. 150–167, DOI: http://dx.doi.org/10.1016/S0022-1694(97)00117-0.

SMHI (2015) Nederbördsintensitet. Available from: https://www.smhi.se/kunskapsbanken/meteorologi/nederbordsintensitet-1.19163 [2019-04-03].

SMHI (2017) Översvämningar. Available from: https://www.smhi.se/kunskapsbanken/hydrologi/oversvamningar-1.5949 [2019-02-04].

Šraj, M., Dirnbek, L. och Brilly, M. (2010). The influence of effective rainfall on modeled runoff hydrograph. *Journal of Hydrology and Hydromechanics*, , vol. 58, DOI: http://dx.doi.org/10.2478/v10098-010-0001-5.

Surkan, A. J. (1974). Simulation of storm velocity effects on flow from distributed channel networks. *Water Resources Research*, , vol. 10, p. 1149–1160, DOI: http://dx.doi.org/10.1029/WR010i006p01149.

Svenskt Vatten (2011). Nederbördsdata vid dimensionering och analys av avloppssystem. *P104*.

Svenskt Vatten (2016). Avledning av dag-, drän- och spillvatten: Del 1 - Policy för funktionskrav för samhällens avvattning.. *P110 - Del 1*.

US EPA (2018) Storm Water Management Model (SWMM). Available from: https://www.epa.gov/water-research/storm-water-management-model-swmm, [2019-01-29].

Vaes, G., Willems, P. och Berlamont, J. (2002) Moving design storms for combined sewer systems. *Global solutions for urban drainage*. , p. 1–15, Portland, United States: American Society of Civil Engineers, DOI: http://dx.doi.org/10.1061/40644(2002)238.

Vägverket (2008). VVMB 310 Hydraulisk Dimensionering. *2008:61*.

Veldhuis, M., Zhou, Z., Yang, L., Liu, S. och Smith, J. (2018). The role of storm scale, position and movement in controlling urban flood response. *Hydrology and Earth System Sciences*, , vol. 22, p. 417–436, DOI: http://dx.doi.org/10.5194/hess-22-417-2018.

Volpi, E., Di Lazzaro, M. och Fiori, A. (2013). Analytical modeling of the hydrologic response under moving rainstorms: Storm–catchment interaction and resonance. *Journal of Hydrology*, , vol. 493, p. 132–139, DOI: http://dx.doi.org/10.1016/j.jhydrol.2013.04.025.

Watt, E. och Marsalek, J. (2013). Critical review of the evolution of the design storm event concept. *Canadian Journal of Civil Engineering*, , vol. 40, p. 105–113, DOI: http://dx.doi.org/10.1139/cjce-2011-0594.

Willems, P. (2001). A Spatial rainfall generator for small spatial scales. *Journal of Hydrology*, , vol. 252, p. 126–144, DOI: http://dx.doi.org/10.1016/S0022-1694(01)00446-2.

Yen, B. C. och Chow, V. T. (1969). A laboratory study of surface runoff due to moving rainstorms. *Water Resources Research*, , vol. 5, p. 989–1006, DOI: http://dx.doi.org/10.1029/WR005i005p00989.

APPENDICES

APPENDIX A MIKE 21 MODEL INPUT

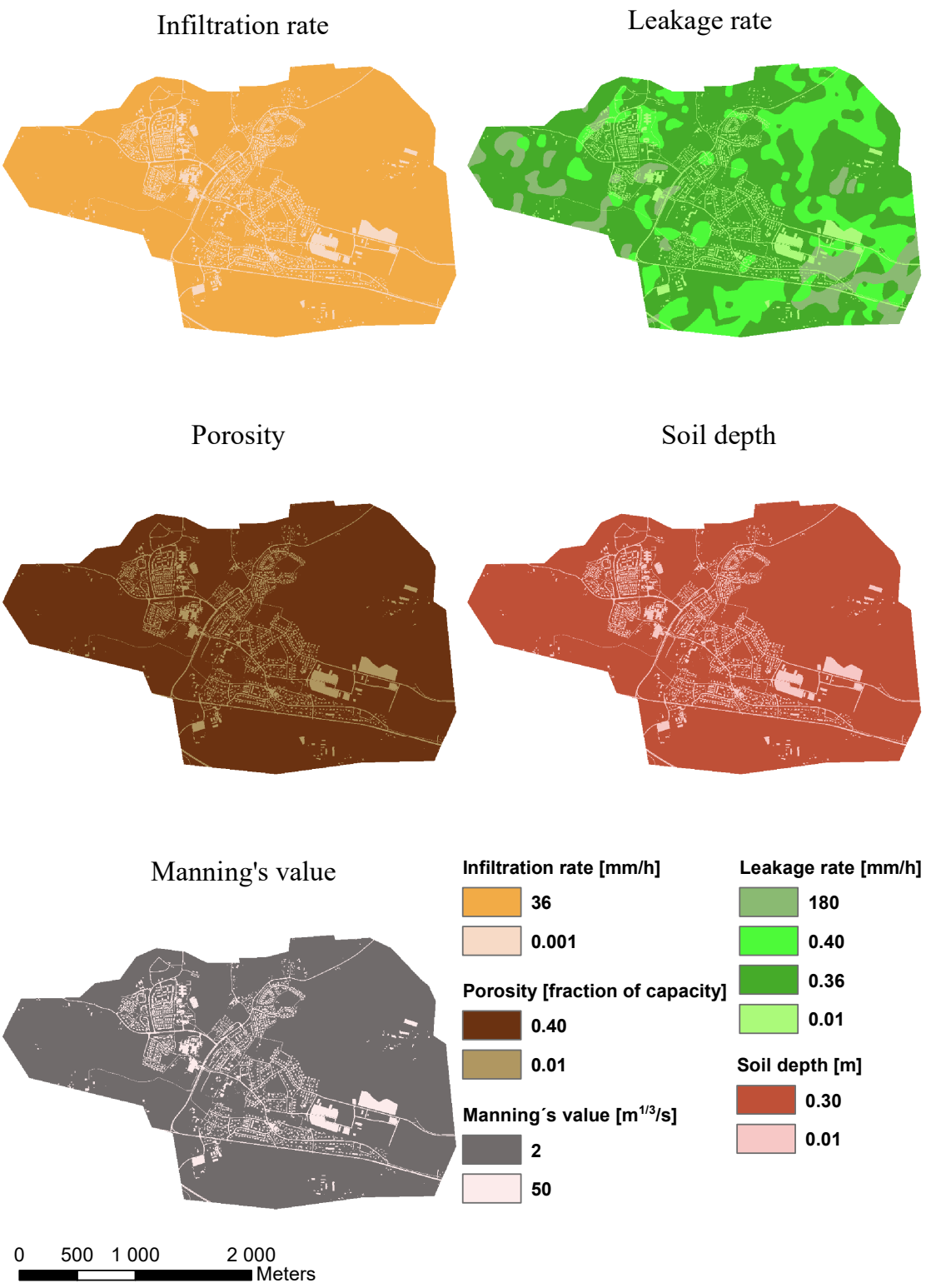

Figure A.1. MIKE 21 model input.

APPENDIX B MAP OF ABSOLUTE DIFFERENCE IN MAXIMUM FLOOD DEPTH

To investigate how well the results at the evaluation points reflect the the whole model domain, a map of the difference in maximum flood depth for the non-moving scenarios with Hyetograph 3 and the CDS-rain was created, see Figure B.1.

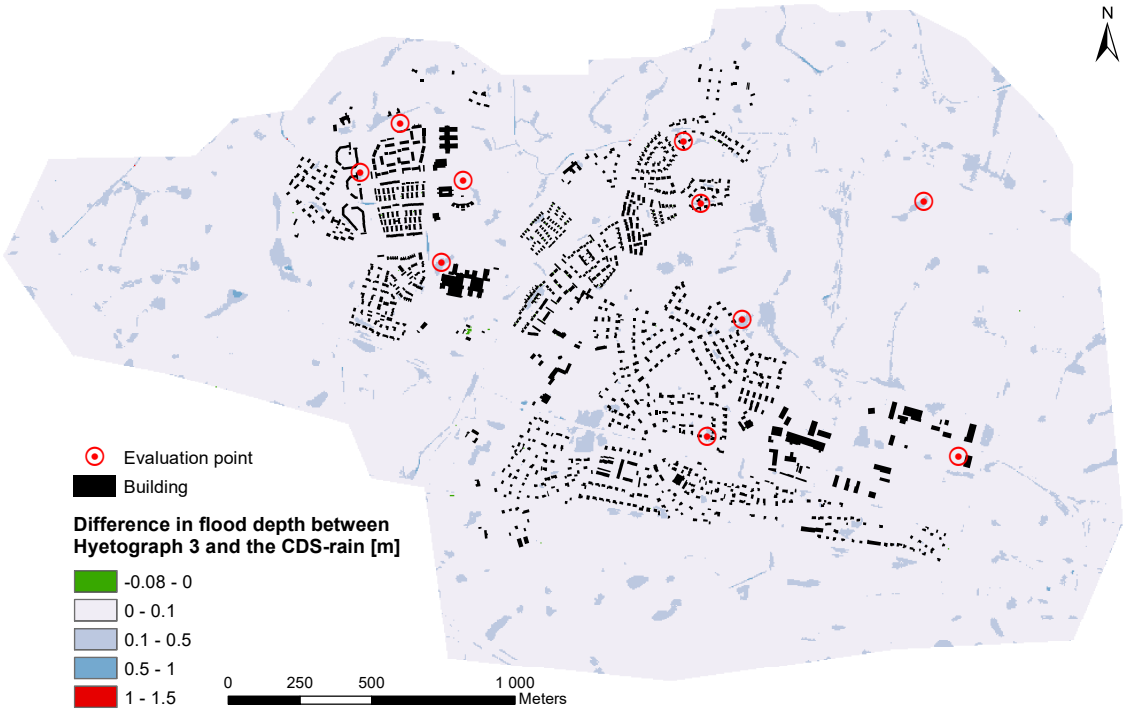

Figure B.1. Absolute difference in maximum flood depth. A positive value indicates that the CDS-rain produces higher water depths and vice verse.

APPENDIX C FLOW SPEEDS

Figure C.1 and C.2 show how the maximum flow speed varies spatially when Hyetograph 1 was simulated with no storm movement. The maps also highlight two selected areas for which weighted means of flow speed were calculated.

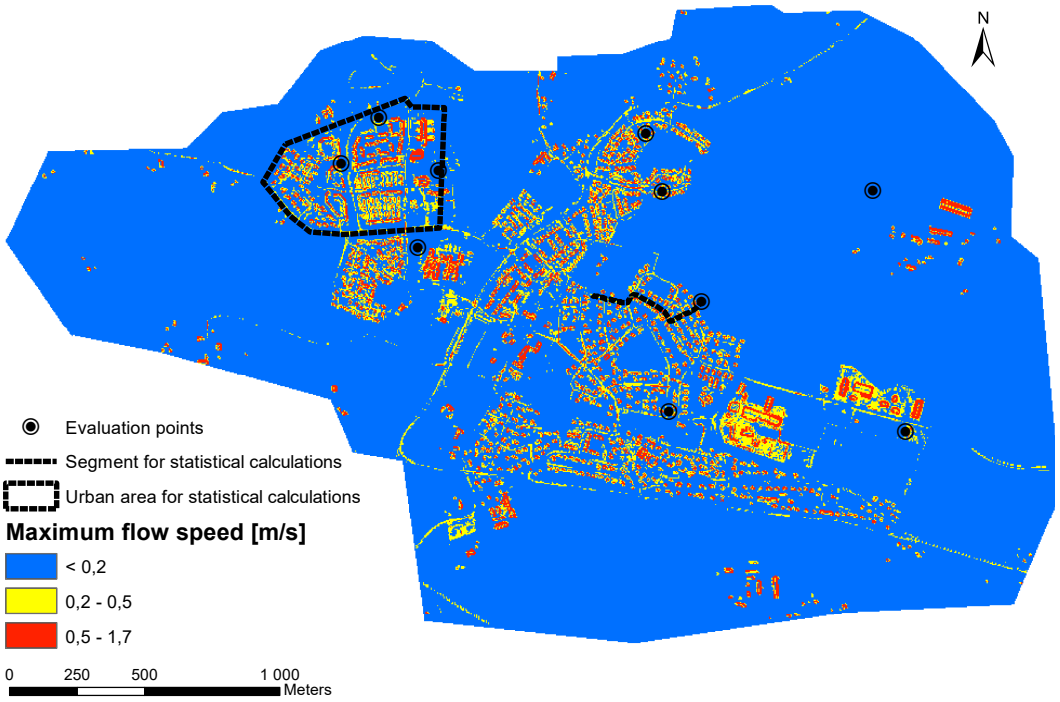

Figure C.1. Maximum flow speed in the whole model domain. The map also shows the evaluation points and the areas for which statistical calculations were performed.

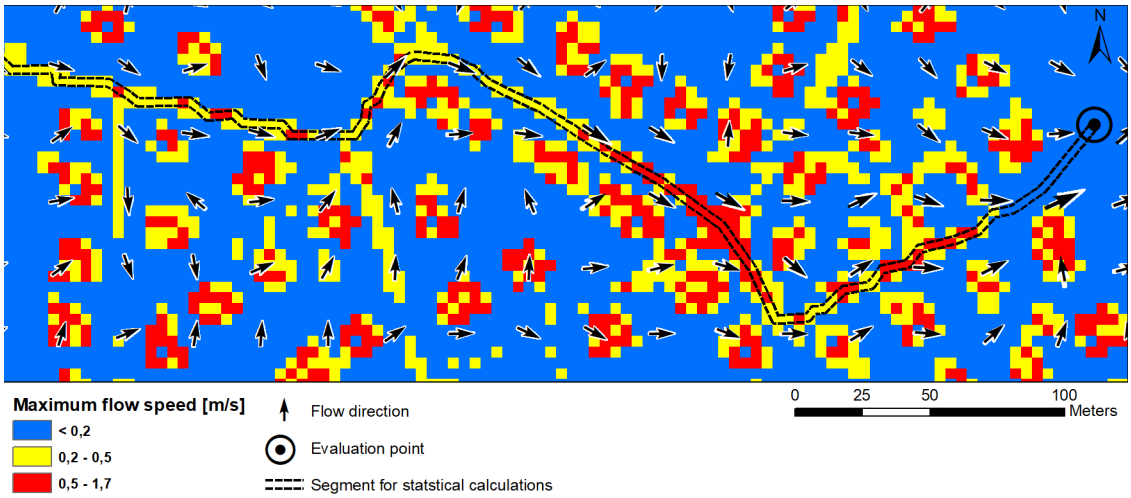

Figure C.2. Maximum flow speed around the upstream segment of evaluation point I. The map also shows the flow direction at maximum flow speed.

The weighted mean of the maximum flow speed ($\overline{v}_{max}$) was defined as

$$\overline{v}_{max} = \frac{\sum_{i=1}^{n} v_{max,i} \cdot J_i}{\sum_{i=1}^{n} J_i} \tag{20}$$

where $v_{max,i}$ (m/s) is the maximum flow speed in grid cell i, J_i (m^3/s/m) is the average horizontal water flux in grid cell i and n is the number of grid cells. The other mean value ($\overline{v}_{60}$), was calculated in the same manner but averaged over the mean flow speed of the first hour ($v_{60,i}$) instead of the maximum speed:

$$\overline{v}_{60} = \frac{\sum_{i=1}^{n} v_{60,i} \cdot J_i}{\sum_{i=1}^{n} J_i} \tag{21}$$

The statistical measures described by Equation 20 and 21 were used for the whole model domain, a delimited urban area and for a segment that is located upstream evaluation point I (Figure C.1 and C.2). Weighted means were calculated for the scenario with Hyetograph 1 and no storm movement and the results are summarized in Table C.1.

Table C.1. Weighted mean of flow speed for the whole model domain, a delimited urban area and for a segment upstream evaluation point I.

	Domain	Urban	Segment
$\overline{V}_{max}$ [m/s]	0.13	0.29	0.45
$\overline{V}_{60}$ [m/s]	0.05	0.10	0.29

APPENDIX D MAPS OF SOIL MOISTURE AT PEAK INTENSITY ARRIVAL

The soil moisture in the model domain at the time before the peak intensity in Hyetograph 1 and 4 arrives is mapped out in Figure D.1. The maps are valid for the non-moving scenario.

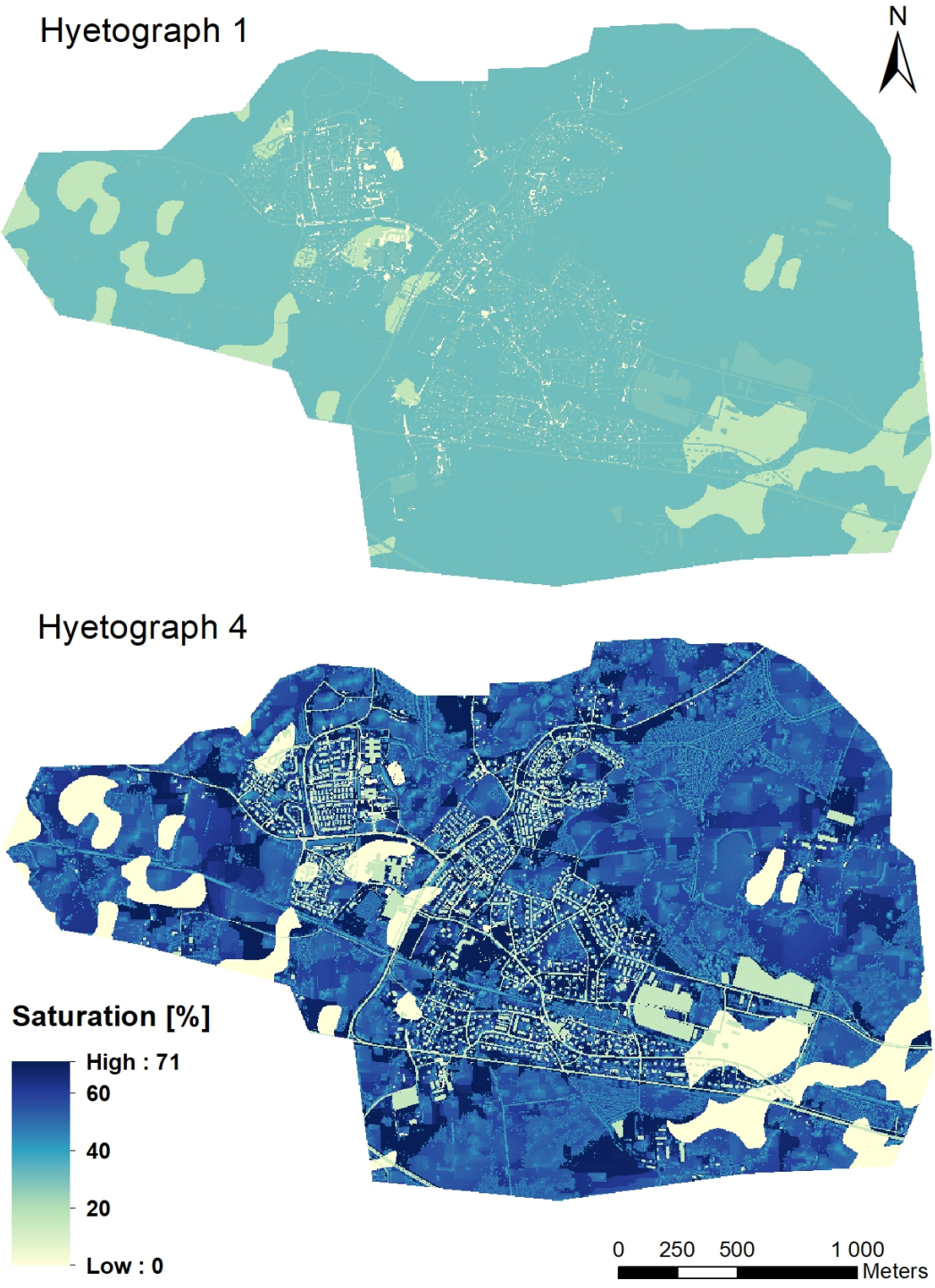

Figure D.1. The degree of soil saturation before the peak in Hyetograph 1 and 4 arrives.

APPENDIX E TIME OF ARRIVAL OF MAXIMUM FLOOD DEPTH IN ALL SCENARIOS

Table E.1. The minute when the maximum flood depth is reached in all scenarios and evaluations points.

	Time arrival of maximum flood depth [min]:									
Scenario	A	B	C	D	E	F	G	H	I	J
1E	120	44	86	53	35	49	81	71	47	86
1W	123	46	89	51	33	44	83	69	46	79
1N	120	44	85	52	33	46	81	69	45	82
1St	119	41	84	48	30	42	78	66	42	78
2E	123	94	125	84	54	78	110	64	74	122
2W	126	94	126	83	54	73	112	63	71	121
2N	124	94	125	83	54	75	111	62	71	118
2St	119	90	121	78	50	72	108	59	69	120
3E	135	135	181	128	99	128	137	113	120	134
3W	138	137	181	126	97	123	139	111	118	129
3N	136	136	181	127	97	125	137	110	117	129
3St	133	132	181	123	94	122	134	108	114	127
4E	181	132	167	135	120	135	150	129	133	144
4W	181	134	170	133	117	130	152	127	131	138
4N	181	133	167	134	119	132	150	126	131	138
3St	181	129	164	130	114	129	147	124	128	137
5E	181	178	181	149	132	151	161	138	147	156
5W	181	180	181	147	131	146	163	136	145	150
5N	181	179	181	148	131	148	161	134	145	150
5St	181	175	181	144	127	144	158	133	142	149
CDSE	124	84	115	92	72	88	115	107	84	118
CDSW	127	87	116	91	70	83	117	105	84	113
CDSN	125	86	115	92	70	85	115	108	84	113
CDSSt	122	82	112	88	67	82	112	102	79	112

APPENDIX F MAXIMUM FLOOD DEPTHS IN ALL SCENARIOS

Table F.1. Maximum flood depth at the evaluation points in all scenarios.

	Flood depth [cm] at evaluation point:									
Scenario	A	B	C	D	E	F	G	H	I	J
1E	43.41	34.04	37.66	49.91	41.11	29.23	40.90	37.05	30.49	29.11
1W	43.41	34.07	37.62	49.88	40.98	29.22	40.84	37.10	30.29	29.13
1N	43.39	34.06	37.63	49.92	41.04	29.22	40.89	37.05	30.43	29.12
1St	43.42	34.06	37.66	49.91	41.05	29.24	40.90	37.10	30.40	29.16
2E	38.15	32.25	33.64	43.93	29.98	22.60	31.56	23.92	22.20	25.26
2W	38.14	32.25	33.60	43.91	29.85	22.60	31.56	23.93	22.12	25.27
2N	38.11	32.27	33.59	43.96	29.92	22.60	31.57	23.92	22.18	25.27
2St	38.17	32.26	33.65	43.97	29.94	22.64	31.60	23.93	22.17	25.34
3E	33.76	29.94	31.08	38.62	21.59	16.00	24.98	22.76	18.33	23.14
3W	33.73	29.97	31.03	38.61	21.43	16.03	24.98	22.75	18.26	23.17
3N	33.65	29.98	31.04	38.66	21.55	15.98	24.94	22.75	18.32	23.17
3St	33.78	29.98	31.16	38.69	21.56	16.10	25.01	22.76	18.33	23.25
4E	39.31	33.12	35.80	47.74	40.65	25.60	35.72	27.30	27.98	27.78
4W	39.27	33.16	35.77	47.72	40.55	25.60	35.74	27.32	27.77	27.80
4N	39.24	33.15	35.78	47.75	40.61	25.60	35.71	27.22	27.92	27.80
4St	39.35	33.14	35.81	47.76	40.62	25.66	35.78	27.32	27.91	27.86
5E	35.57	31.35	32.62	42.95	36.60	20.64	28.94	23.57	23.13	25.30
5W	35.50	31.34	32.55	42.94	36.41	20.65	28.96	23.57	22.91	25.32
5N	35.47	31.34	32.58	42.98	36.49	20.63	28.92	23.55	23.05	25.32
5St	35.64	31.35	32.69	43.00	36.52	20.70	28.99	23.57	23.05	25.42
CDSE	45.00	34.34	39.23	51.07	41.71	28.53	41.76	37.24	30.81	30.63
CDSW	44.98	34.36	39.17	51.04	41.66	28.48	41.67	37.30	30.73	30.60
CDSN	45.00	34.36	39.17	51.08	41.69	28.49	41.73	37.21	30.81	30.62
CDSSt	45.01	34.35	39.20	51.07	41.69	28.49	41.72	37.27	30.79	30.64

APPENDIX G FLOOD DEPTH VERSUS TIME AT ALL EVALUATION POINTS

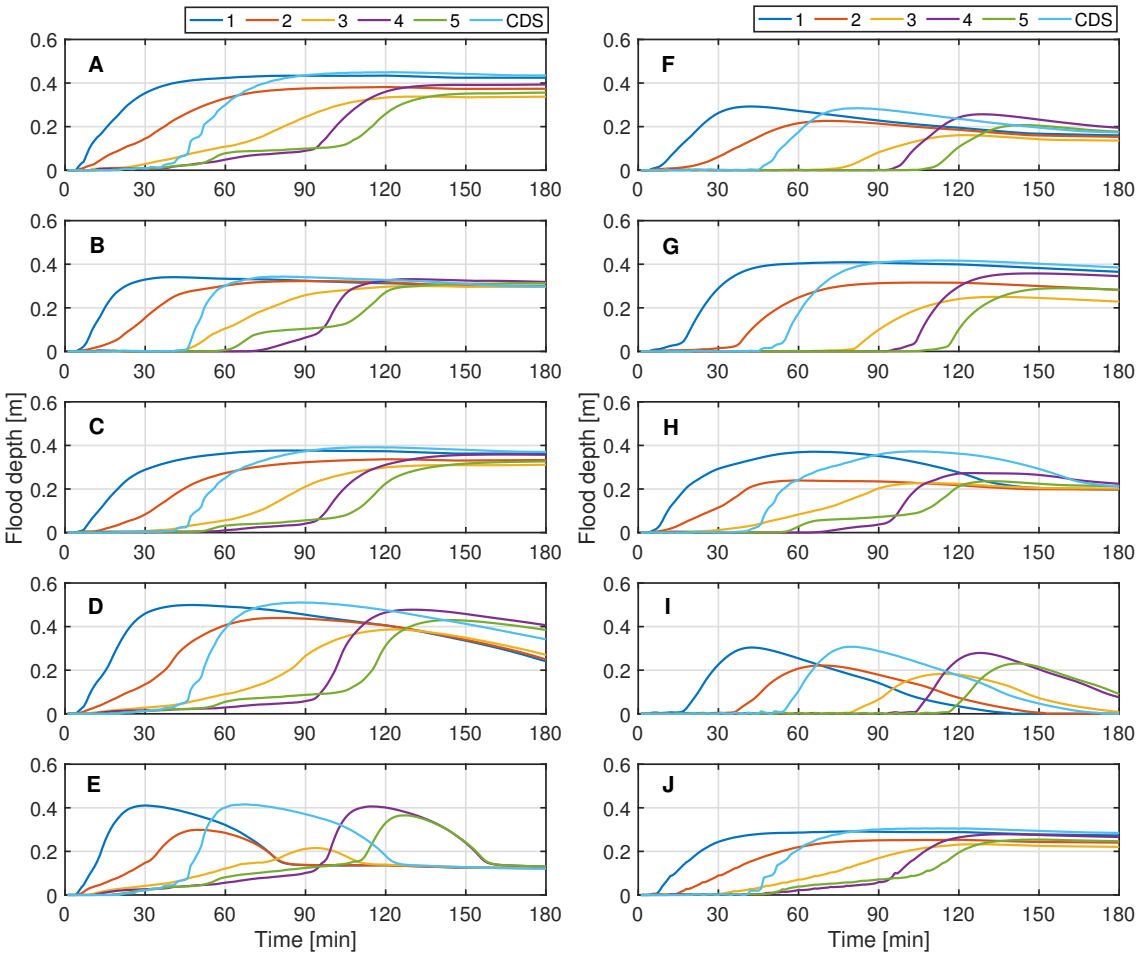

(a). Evaluation point A–E.

(b). Evaluation point F–J.

Figure G.1. Flood depth as a function of time at all evaluation points for all hyetographs with a non-moving scenario.

APPENDIX H WATER LEVEL CORRECTION

Table H.1. The amount of artificially generated water (to maintain model stability) in the MIKE 21 (M21) and MIKE URBAN (MU) model.

	Water level correction [m^3]	
Scenario	M21	MU
1E	37238	3040
1W	37633	2923
1N	37381	2979
1St	35367	2615
2E	25795	4996
2W	26052	5015
2N	25871	4976
2St	24814	4638
3E	21811	8721
3W	21872	8853
3N	21821	8720
3St	21021	8398
4E	45922	10795
4W	46289	10799
4N	46218	10771
4St	43114	10437
5E	38660	11241
5W	38959	11122
5N	38898	11142
5St	36973	10787
CDSE	23072	6419
CDSW	23112	6314
CDSN	23106	6363
CDSSt	22892	6000